Applied Technologies

Verification and Validation Report for ATBM Torso Finite Element Model

Technical Report J0511-18-724
Under Prime Contract N00174-17-C-0003

Prepared by
Laurel Ng, Ph.D.
Eugene Niu, Ph.D.

L-3 Applied Technologies, Inc.
10180 Barnes Canyon Rd. Suite 100
San Diego, California 92121

Prepared for
Terri Schull
2807 Strauss Avenue
Bldg. 695, Code R3C
Indian Head, MD 20640

December 12, 2018

Document Version

Date	November 5, 2018
Program	HEMAP
Program Sponsor	JNLWD
Document Title	Verification and Validation Report for ATBM Torso Finite Element Modeling
Document Type	V&V Report
M&S Name & Version	1.0
Document Version	1.0
Prepared by:	Eugene Niu
Distribution Statement	Distribution Statement A
Classification	Unclassified

Record of Changes

Version	Date	Changes
1.0	10/17/2018	First draft
2	11/5/2018	Final draft
3	12/12/2018	Final with Dist A statement

Contents

Figures

Tables

1 Executive Summary

This report documents the completed verification and validation (V&V) activities for the 360° human torso (includes the back) finite element model (FEM) as part of the blunt trauma Modeling and Simulation (M&S) program known as the Advanced Total Body Model (ATBM). The report details the specific requirements, acceptability criteria, and analysis methods used to validate the model's data, conceptual model, and results, as well as verify its data, design, and implementation. The report summarizes the activities used to identify, evaluate, and quantify any limitations of the M&S as well as any risks associated with its use.

The ATBM program was developed in the mid-2000s for use by the Joint Non-Lethal Weapons Directorate (JNLWD) as an analytical tool to estimate the risk of injuries from Kinetic Energy NLWs (KE-NLWs). In 2006, a thoracic model was the first component of ATBM completed and included injury correlates of rib fracture and lung contusion. Models of the head, eye, upper abdomen, face, extremities, lower abdomen, and neck were developed in subsequent years. The lower abdomen FEM was developed, verified and validated during 2014 to 2016 and the neck FEM was delivered in 2017. In 2018, the improved 360° human torso FEM, which includes the 3D spine, is developed.

The human torso FEM is being developed for the purpose of accurately predicting the responses to blunt impacts, including subject motion, stresses, and strains of the torso region spanning from the lower neck (vertebrae C5) to the middle waist (vertebrae L5). The model is formed from anatomically accurate geometry of the 50th percentile male (Zygote 3D Male Human Model, Zygote Media Group, American Fork, UT), discretized at the organ level with finite elements, and assigned tissue material models based on literature sources and test data. Impacts between the torso and a projectile are simulated with the LS-Dyna nonlinear explicit solver, providing model responses that can be correlated to injury outcomes.

The scope of the V&V Report covers the human torso and back FEM development. The requirements of the M&S were determined by the subject matter experts (SMEs) developing the M&S to meet the capabilities needed by the M&S sponsor. The limitations and risks of the M&S are dependent upon the available resources, such as literature data, but are a consequence of the simplifications required by FEA. Because many of the V&V activities were conducted in parallel with the M&S development, these limits and risks were identified in the course of planned V&V activities, rather than prior to model development.

Concept validation is the process to confirm that the chosen abstraction types (in this case finite element modeling) are adequate representations of the observed phenomena. Assessing the FEM's geometry, mesh quality, material models, and parameter sensitivity are all methods that can evaluate the choice of using the finite element method and reduce uncertainty in the model.

Two activities were performed as part of the FEM's design verification: 1) a check of the model's geometrical and inertial properties and 2) mesh convergence studies. The former activity tested whether the organ meshes occupy the intended region of space, while the latter confirmed that the mesh has the appropriate level of discretization, or *mesh density*. Mesh convergence studies reduce the computational cost of running the M&S by finding an optimal number of nodes and elements that produce satisfactory results.

Implementation verification activities were focused on ensuring that the FEM components have been integrated correctly. Various model checks, such as unconstrained modal analyses and energy checks were performed incrementally during the model development. Any problems that arose during these tests often uncover problems in the model's design and were fixed prior to further development. Some of the model's test cases are performed in every instance of running the M&S and become the basis for defining the model's limitations.

Results validation is the final stage in the V&V process. Predictions from the two components of the M&S—the FEM and its injury correlations—were compared against test data. In general, contact force curves can be generated by the FEM and plotted against the measured impact force of projectiles.

The aforementioned V&V activities were completed in 2018. The primary limitation of the effort was finding enough relevant data to conduct the results validation. This report also documents any technical challenges the M&S developer had to completing various V&V activities.

2 Problem Statement

The modeling and simulation (M&S) was created to predict the *human effects* of blunt trauma to the torso and, more specifically, answer the following questions:

1. How does the torso of a human respond to the blunt impact of a kinetic energy non-lethal weapon (KE-NLW)?
2. What types of injuries will be incurred by blunt impact to the torso, including the back region?
3. How severe will those injuries be to the torso?
4. What is the likelihood of incurring each injury type?

The M&S simulates the mechanical responses and interaction between the blunt impactor and the tissue of the torso. The body's responses to that impact, such as how the load becomes distributed, the internal deformation of each organ, and the stress state of those organs are computed by the M&S. That information is coupled to empirically-derived dose-response curves to predict the type, severity, and likelihood of an injury to each organ at torso region.

The results of the M&S will guide decision-making at several stages of the acquisition process for KE-NLWs. During Development Test and Evaluation (DT&E), the M&S can evaluate the human effects of various KE-NLW design concepts or prototypes and indicate which design modifications yield the desired human effects. In the latter stages of the acquisition process, such as Operational Test and Evaluation (OT&E), the M&S can predict the Risk of Significant Injury (RSI) of the NLW system in various operational scenarios.

The results of this M&S are a critical part of the programmatic decisions made for a NLW system acquisition process; inaccurate predictions can result in several adverse consequences. An evaluation that overstates the injury risks could force the developing agency into reengineering (in design, operation, or implementation) the NLW system to be safer. Likewise, if an evaluation understates the injury risks, a program could progress far into the latter stages of the acquisition process before the discovering a critical design flaw. Mitigating these issues during OT&E or later would be significantly costly. Furthermore, the deployment, operational usage, and training of the NLWS rely upon an accurate representation of the risks involved with its use. Significant inaccuracies could lead to the NLWS being rendered ineffective or excessively harmful when in actual use.

2.1 Intended Use

The M&S provides the capability to assess probability of injury to torso organs by simulating the impact between a NLW projectile and the human torso. The probabilities of various injury occurrences are correlated to the torso's responses to a NLW impact and the damage limits of the associated tissues. The model is also intended to give guidance regarding the development of new non-lethal projectiles during their design phase, thereby allowing developers to modify their

designs to prevent unacceptable levels of injury while still yielding the desired effects on the targeted individuals.

2.2 Modeling and Simulation (M&S) Overview

The M&S for which this report is written is a finite element model (FEM) that simulates the solid mechanics of a blunt impact to the human torso combined with mechanical responses that use the FEM outputs to predict the occurrences of several types of torso injuries. The FEM includes the torso anatomy beginning from the lower neck (vertebrae C5) and extending downward to the middle waist (vertebrae L5). Only key anatomical features have been incorporated into the torso FEM: the spine (vertebrae, disc, facet joints, ligaments), ribs, costal cartilage, sternums, lungs, liver, spleen, stomach, kidneys, heart, and a body exterior tissue (a homogeneous tissue representing the muscle, fat & skin). All other anatomical features (e.g., tendons, small ligaments, and small blood vessels) were not included for simplicity.

Configuration control of the M&S is maintained by documenting the changelog of each FEM. Detailed M&S information is provided in Appendix A.

2.3 M&S Application

This subsection describes how the M&S will be used in the overall program and lists the program objectives that the M&S should meet in order to fulfill the intended use.

The M&S is one of several FEMs that model the biomechanics of blunt trauma, each dedicated to a specific region of the body. This collection, the Advanced Total Body Model (ATBM), is itself part of a larger software application called the Human Effects Modeling Analysis Program, which is used to evaluate the human effects of all types of non-lethal stimuli including blast, thermal, auditory, flash-blindness, and underwater acoustics.

The human torso FEM, in conjunction with the rest of ATBM, can be used to conduct risk assessments of blunt impacts to torso (frontal and rear) regions of the body. The output of ATBM is in the form of the probability of incurring certain injury types such as bone fractures or organ lacerations/ruptures. ATBM's output can then be aggregated into a final RSI that takes into account the relative severities of each injury type, the possibility of incurring more than one injury at a time, and the projectile's accuracy and velocity at a particular range.

2.4 Accreditation Scope

The interest of the Joint Non-Lethal Weapons Directorate (JNLWD) in assessing the NLWs procured in the future has led to the need to assess the injury risks of body impacts. The scope of the accreditation effort will include a detailed review of this Verification and Validation (V&V) report as well as supporting documentation to determine if the torso FEM and associated injury correlates reliably and accurately represent existing data on torso impacts from NL projectiles.

2.5 V&V Scope

This subsection describes the scope of the V&V effort based on the assessment of M&S requirements, acceptability criteria, and the availability of resources. The accuracy of the human torso model and associated injury correlations are assessed by its ability to calculate a FEM response that sufficiently predicts both the projectile motion from high-speed impacts to the torso and the likelihood that the impact will cause injury.

3 M&S Requirements, Assumptions, Capabilities, Limitations, & Risks/Impacts

This section describes known factors that constrain the development and/or use of the M&S or that impede the VV&A effort, including the model requirements, assumptions, capabilities, limitations, and risk factors affecting M&S development and risks associated with using the M&S for the intended use.

3.1 M&S Requirements and Acceptability Criteria

This section describes the M&S requirements defined for the intended use, the derived acceptability criteria that should be met to satisfy the requirements, the quantitative and qualitative metrics used to measure their success, and are sequenced in the order in which they are listed in the model development requirement (Niu and Ng 2018). Table 3-1 lists the relevant requirements and acceptability criteria for the components of the FEM (such as individual organs and referred to as sub-systems). Table 3-2 lists requirements and acceptability criteria for the FEM as a whole.

Table 3-1. List of requirements and acceptability criteria for M&S FEM sub-systems.

Req. #	Requirement	Necessary criteria	Preferred criteria
3.1.1.1	Each sub-system will be meshed such that it contains the critical anatomical details necessary for accurate load transmission between adjacent sub-systems. Minor geometric details will be omitted (Anatomical geometry accuracy).	FE mesh of each organ/part must match reference geometry volume or area within 10%	FE mesh of each organ/part must match reference geometry volume or area within 5%
3.1.1.2	Each sub-system mesh resolution will be enough to ensure convergence of simulation results (Mesh convergence).	Volume percentage of peak mechanical responses (stress, strain, energy) match well those from finer mesh model.	Peak mechanical responses (stress, strain, energy) match finer mesh within 5% at same locations.
3.1.1.3	The material properties of the organs conform to the available test data within the deformation and strain-rate regimes of interest (Material model sensitivity)	Each organ's material model conforms with established stress-strain corridors from published test data	Material model covers the strain-rate response of application and its response will be within the dynamic regimes of interest
3.1.1.4	Injury correlates shall be derived directly from the tissue mechanical responses of the associated sub-system (Injury correlation)	Ultimate strength will be directly used as a threshold to determine the injury, if sufficient data is not available to establish regressions	Injury regression will be established statistically using tissue-level responses (stress, strain, or energy)

Table 3-2. List of requirements and acceptability criteria for integrated FEM.

Req. #	Requirement	Necessary criteria	Preferred criteria

3.1.2.1	No spatial penetration exists between sub-systems (Model construction & assembly)	Penetration due to mismatch of mesh resolution will be avoided be specifying appropriate contact formulations	Model passes penetration checks in LS Pre-/Post and has no warnings during simulation initialization
3.1.2.2	No big gaps between internal organs and chest wall, among contact organs (Model construction & assembly)	Adjust surface of internal organs to contact chest wall	None
3.1.2.3	All contact and boundary conditions are properly initialized before the simulation (Model initialization)	The model has no internal energy at the beginning of the simulation	None
3.1.2.4	Material model parameters proportionally affect simulation results (Model sensitivity)	20% perturbations in critical material property parameters result in a 20% or less proportional change in response	None
3.1.2.5	Hourglass energy is minimal and limited throughout the simulation (Energy convergence)	Total hourglass energy less than 10% of the initial system energy in any test case	Total hourglass energy less than 5% of initial system energy in any test case
3.1.2.6	Model maintains its integrity with minimal number of deleted elements due to excessive deformation (Model computational stability)	Fewer than 5% of elements deleted due to negative volume in all test cases	Fewer than 1% of elements deleted due to negative volume in all test cases
3.1.2.7	Simulations of assembled model produce results comparable to those found in literature (Model validation)	Model compares favorably with published data of thorax dynamics caused by blunt impact, such as peak forces and deflection	Force-deflection results from simulations reside within corridors established from test data
3.1.2.8	Model produces accurate injury outcomes (Correlation validation)	Injury predictions from simulations of tests match published data statistically	None
3.1.2.9	Model based upon a 50% male but can be enlarged to a 95% male and reduced to a 5% male (Model adaptability & flexibility)	Simulation results from scaled models compare favorably with test data; computation completes within 150% runtime of 50% male model	None

3.2 M&S Assumptions

This subsection describes the known assumptions about the M&S and the data used in support of the M&S in the context of the problem:

- The geometry is taken from the Zygote 3D Male Human Model (Zygote Media Group, American Fork, UT), which is assumed to be representative of a 50th percentile male.

- The FEM contains tissue (flesh (muscle, skin), organs, and bones). Each organ is treated as one continuum with uniform material properties contacting adjacent organs with sliding surface contact definitions.
- The necessary anatomical simplifications made to generate the FEM have a negligible effect on the relevant model outputs.
- Material properties are assigned based on available literature data, which are assumed to represent average tissue properties for the human population.

3.3 M&S Capabilities

The M&S can calculate both gross and micro-level dynamic responses of a 50th percentile male's torso under high-speed NLW-relevant blunt impacts. The responses are tied to model-specific injury correlates to predict the probability of injuries to the organs within the torso region.

3.4 M&S Limitations

This subsection describes the known constraints and limitations associated with the development, testing, and/or use of the M&S. These constraints and limitations may be introduced as a result of an ongoing development process or may result from information garnered in previous VV&A efforts.

Since there are no yield, failure, or damage properties defined in the FEM, the model is limited to calculating the dynamic responses of impacts without material failure. Predicting the response of the torso after damage to an organ or the severity of the injury of the organ is beyond the present scope of the model in its current state.

The model either excludes or simplifies certain anatomical elements such as minor blood vessels, tendons, small ligaments, and minor cartilage. Thus, predicting responses or injuries to these elements is outside the scope of the model's intended purpose.

Although the FEM is designed to complete all simulations during model construction and validation, abnormal termination due to element inversion or numerically infinite nodal velocities may be possible for more severe ballistic impacts associated significant large deformation.

The degree to which validation efforts can be undertaken is a function of the available resources, particularly the available data from post-mortem human subject (PMHS) tests. As the supply of data becomes exhausted, the validation of certain M&S components may remain incomplete or strictly qualitative.

3.5 M&S Risks/Impacts

This subsection describes the known risks associated with the development and/or use of the M&S within the context of the application. The model's capabilities are predicated on the

available geometric and material properties as well as all necessary simplifying assumptions. In this case, the FEM is developed from a commercially-available geometry of a male body (Zygote 3D Male Human Model (Zygote Media Group, American Fork, UT)) and assigned properties based on available literature data.

The results are most reliable for a person with the geometry and material properties that most closely match the FEM. Due to the large geometric and material variation in these features within the global population, injury estimates may differ significantly on a case-by-case basis.

4 V&V Task Analysis

This section provides an overview of the results of the V&V inspection and testing activities, as outlined below. Included are details regarding any deviations from the V&V Plan and the justification for each change as well as all sources of data and any applicable quality-assurance documentation. Table 4-1 maps each requirement of the M&S to its associated V&V activity (Table 3-1 and Table 3-2). Any modifications from the V&V Plan's method or acceptability criteria are summarized in the corresponding notes.

Table 4-1. V&V activity conducted for each requirement.

Req. #	M&S Requirement Description	V&V Activity Type and Report Section	Notes	Status (Failed, Necessary, Preferred)
3.1.1.1	*Anatomical geometry accuracy.* Each sub-system will be meshed such that it contains the critical anatomical details necessary for accurate load transmission between adjacent sub-systems. Minor geometric details will be omitted.	Conceptual Validation (Section 4.2.1)	Adjust internal organs to reduce gaps	Necessary
3.1.1.2	*Mesh convergence.* Each sub-system mesh resolution will be enough to ensure convergence of simulation results.	Design Verification (Section 4.3.2)	No modification	Necessary
3.1.1.3	*Material model sensitivity.* The material properties of the organs conform to the available test data within the deformation and strain-rate regimes of interest.	Conceptual Validation (Section 4.2.3)	Use overall data and adjust to match test data	Preferred
3.1.1.4	Injury correlates shall be derived directly from the tissue mechanical responses of the associated sub-system (Injury correlation)	Data Verification (Section 4.1.1.7) Result Validation (Section 4.5.5)	No data to develop correlation, limit data to validate injury occurrences	Necessary
3.1.2.1	No spatial penetration exists between sub-systems (Model	Conceptual Validation (Section 4.4.1)	Small penetrations ignored by	Preferred

	construction & assembly)		contact algorithm	
3.1.2.2	No big gaps between internal organs and chest wall, among contact organs (Model construction & assembly)	Conceptual Validation (Section 4.2.1)	No modification	Preferred
3.1.2.3	All contact and boundary conditions are properly initialized before the simulation (Model initialization)	Design Verification (Section 4.3.3)	No modification	Preferred
3.1.2.4	Material model parameters proportionally affect simulation results (Material sensitivity)	Design Verification (Section 4.3.1)	A separate study conduct on material uncertainty.	Preferred
3.1.2.5	Hourglass energy is minimal and limited throughout the simulation (Energy convergence)	Design Verification (Section 4.3.3)	Not existed due to mesh technology	Preferred
3.1.2.6	Model maintains its integrity with minimal number of deleted elements due to excessive deformation (Computational stability)	Result Validation (Section 4.3.3)	No modification	Preferred
3.1.2.7	Simulations of assembled model produce results comparable to those found in literature (Model validation)	Result Validation (Section 4.5.1, 4.5.2, 4.5.3, 4.5.4)	No modification	Preferred
3.1.2.8	Model produces accurate injury outcomes (Correlation validation)	Result Validation (Section 4.5.5)	Limit tests	Necessary
3.1.2.9	Model based upon a 50% male but can be enlarged to a 95% male and reduced to a 5% male (Model adaptability & flexibility)	Result Validation (Section 4.5.1, 4.5.2, 4.5.3, 4.5.4)	Scaling models to match test subject	Necessary

4.1 Data V&V Task Analysis

4.1.1 Data Verification Task Analysis

4.1.1.1 Anatomical Geometry

The human torso FE model consists of two groups, chest wall and internal organs. The internal organs include lungs, heart, liver, spleen, stomach, kidneys, pancreas and intestine. The chest wall includes bones and body exterior tissue, where the bones are composed by shoulder bones (scapula, clavicle, humerus) and ribcage including spine (vertebrae, disc, facet-joint, ligament), ribs, costal-cartilages and sternum. The body exterior tissue is the combination of muscle, skin, fat and other small tissue (blood vessel, ligament, etc.). The polygonal surfaces of geometry were exported from Zygote 3D Male Human Model (Zygote Media Group, American Fork, UT). The surfaces were imported into HyperMesh and geometry cleaning was conducted to remove small complex details. Figure 4-1 depicted the exported surfaces of ribcage, internal organs, skin and torso muscle from Zygote Model. The body exterior tissue is assumed to be a homogenous bulk which geometry is constructed from skin and ribcage external surface, thus the individual muscles are not modeled separately and the body muscle geometry shown in Figure 4-1 is not used in model construction.

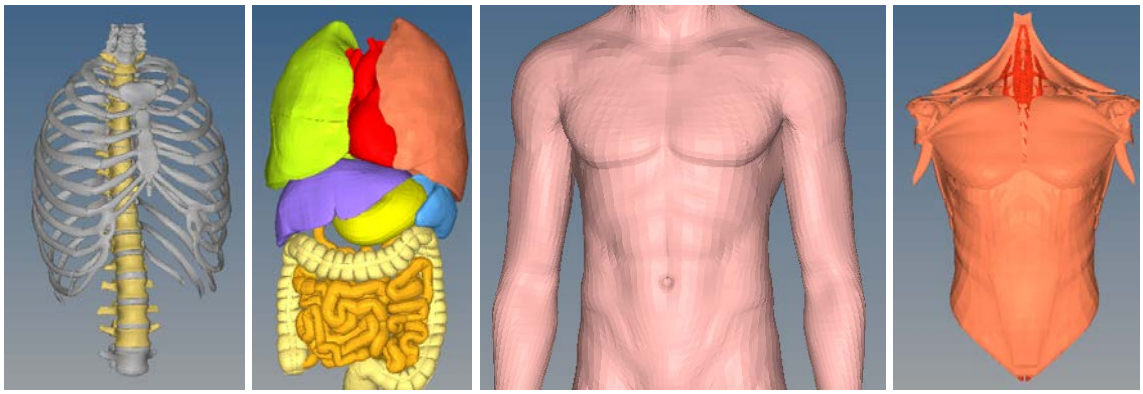

Figure 4-1. Ribcage, internal organs, skin and body muscle exported from Zygote.

4.1.1.2 MCW PMHS Impact Tests

The PMHS impact tests were conduct in 2017 at the Medical College of Wisconsin. The projectiles weighed between 62.6 and 72.9 grams, impact speeds were ranging from 67.3-86.4 m/s and the subject weighted between 50 and 75kg. There are four, three and seven tests which impactor struck on intestine, stomach and kidney, respectively. Table 4-2 summarizes the PMHS impact tests and the impact forces history are given in Figure 4-2.

Table 4-2. MCW PMHS impact test.

Test Name	Impact Location	Projectile mass (g)	Impact Speed (m/s)	PMHS Weight (kg)
S2T2	Intestine	64.7	72.4	64

S4T2	Intestine	71.1	69.1	50
S5T2	Intestine	72.3	68.2	65
S7T2	Intestine	69.6	81.1	65.8
S2T3	Stomach	62.6	67.4	64
S4T3	Stomach	73.0	68.7	50
S7T3	Stomach	69.6	81.1	65.8
S3T1	Left Kidney	65.3	70.7	69
S4T6	Right Kidney	70.1	71.6	50
S6T1	Left Kidney	71.89	86.4	75
S2T1	Left Kidney	63.3	71.3	64
S3T2	Right Kidney	65.3	68.8	69
S5T1	Left Kidney	72.9	70.6	65
S7T1	Right Kidney	71.5	79.7	65.8
S3T1	Left Kidney	65.3	70.7	69
S4T6	Right Kidney	70.1	71.6	50
S6T1	Left Kidney	71.89	86.4	75

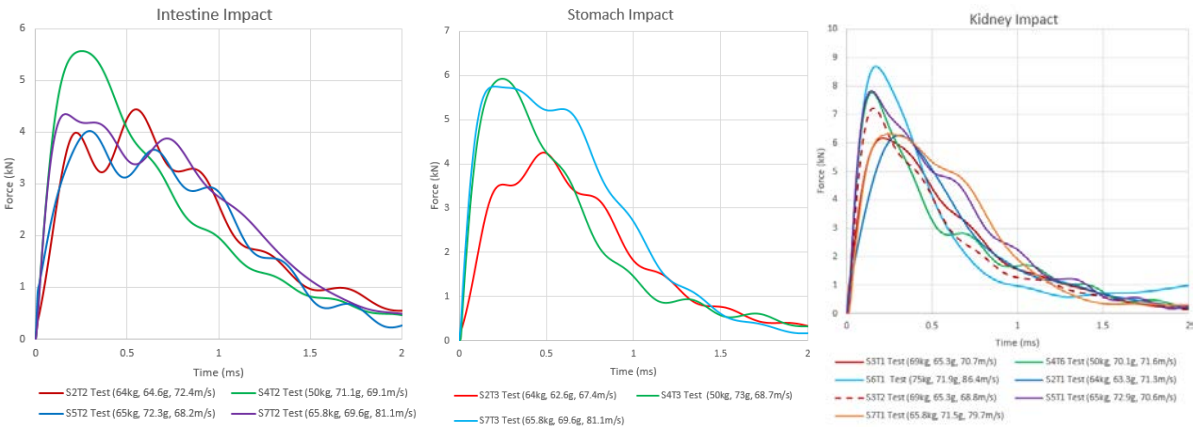

Figure 4-2. Impact forces history on intestine, stomach and kidney

4.1.1.3 Johns Hopkins APL PMHS Tests

The frontal impact tests on PMHS were conducted at Johns Hopkins APL in 2018. A 20mm-diameter cylindrical silicone projectile, weighted 50 grams, was used to impact left rib #4 anterior side at speed 40m/s. Two test conditions were conducted, fleshed and defleshed, where fleshed means the PMHS fleshed was intact over the impact area, while defleshed the PMHS fleshed was removed, shown in Figure 4-3. There were 19 accelerometers and 12 strain gauges used to collect test data. The velocity history obtained from accelerometer placed on the side of the rib opposite of impact (internal surface) and strain from the strain gauge closed to the impact point were plotted at Figure 4-4.

Figure 4-3. APL impact tests with fleshed and defleshed chest wall tissue.

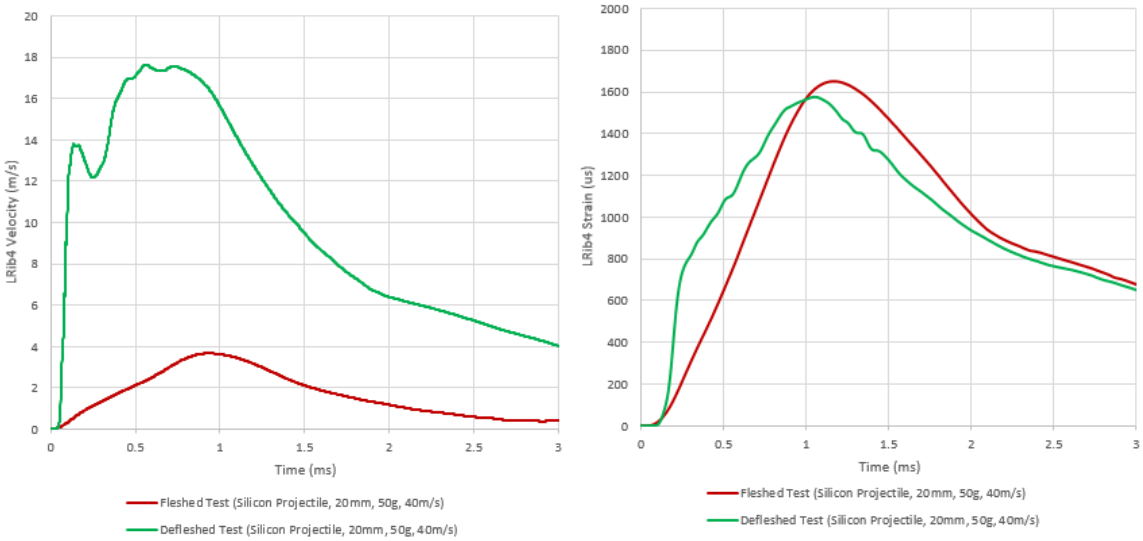

Figure 4-4. Rib velocity and strain history of fleshed and defleshed APL PMHS tests.

4.1.1.4 PMHS Frontal Impact Tests

A serial of PMHS tests were conducted by Kroell, Schneider et al. (1971), (1974). The pneumatic impactors with a diameter of 150 mm were used and were centered at approximately the mid-sternum level. The mass of the impactor ranged from 1.6 to 23.6 kg and the impact velocities, from 4.0 to 14.5 m/s. Two tests on subject 26FM (64kg) and 28FM (68kg) with small impact mass (1.9kg and 1.6kg), high speeds (11.2 and 14,5m/s) and no observed injury can be used to validate developed FE model. The force history for the two tests were given in Figure 4-5.

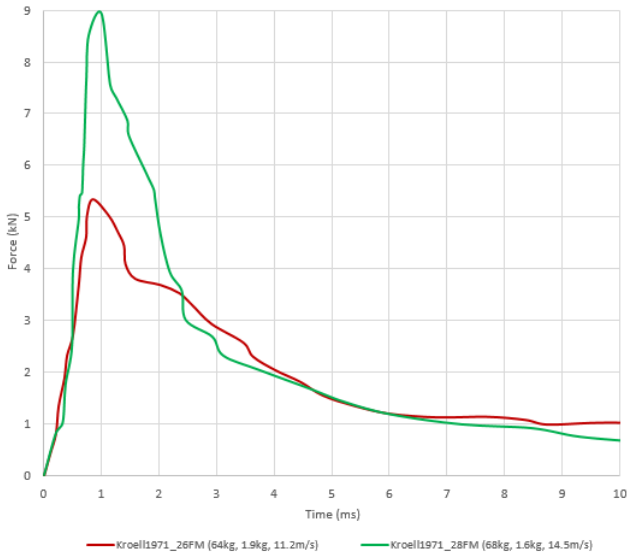

Figure 4-5. Force history of frontal PMHS tests.

4.1.1.5 Back PMHS Impact Test

Forman, Perry et al. (2015) conducted a series of repeated hub impact tests using four male cadavers. Tests consisted of impacting each specimen with a rigid, instrumented hub (15.24cm diameter, 1.27cm radius edge fillet) on the posterior surface of the mid- thorax at approximately the superior–inferior location of the eighth thoracic vertebra (T8). The force-deflection curve of test C9 (subject C and test #8, speed 5.5m/s) was plotted at Figure 4-6.

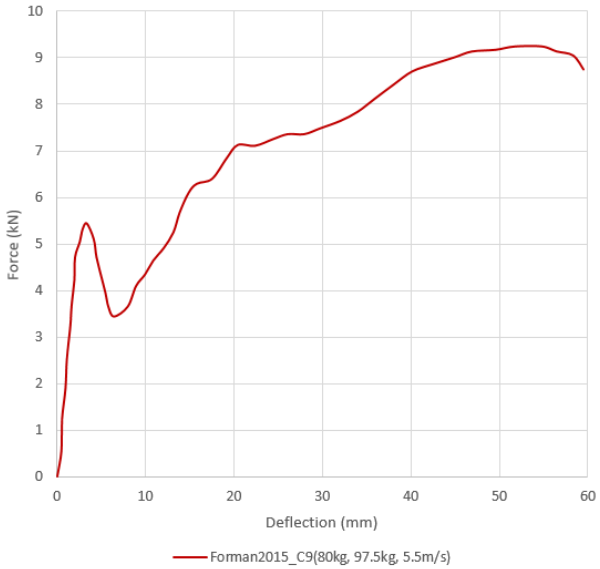

Figure 4-6. Force-deflection curve of back PMHS impact test.

4.1.1.6 Back Drop Test on Animals

Bass, Rafaels et al. (2008) used cadaveric porcine specimens as a model for direct spinal impact injuries to humans to determine an appropriate injury tolerance value. Four porcine cadaver specimens were subjected to five impacts each on the dorsal surface of their lower thorax and abdomen. A schematic diagram of the test fixture is shown in Figure 4-7. The impactor contact surface had a cylindrical profile with a radius of 12.7mm and a length of 80mm. The average drop velocity was measured to be 4.1±0.08 m/s. The peak reaction forces varied from 2400 to 7100 N, and the loading rate varied from 42 to 581 kN/s. Injury occurrences of two thorax back drop tests were listed in Table 4-3.

Table 4-3. Observed Injuries in drop tests on animal back.

Test #	Drop mass (kg)	Drop Velocity (m/s)	Location	Injury
2.1	28	4.2	T7/T8	Spinous process and endplate fracture
4.1	19.1	4.1	T8	Spinous process and endplate fracture

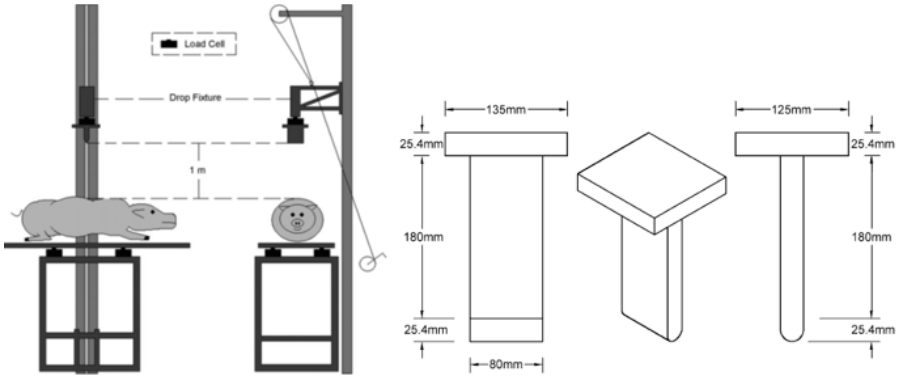

Figure 4-7. Drop test fixture and impactor for porcine specimen.

4.1.1.7 Failure Strength of Spine Organs at Tissue Level

Tissue-level failure strengths and their ranges for vertebrae, disc and facet joint are given in Table 4-4. Stress was selected as common indicator for these spine tissue. Stress values were obtained from tissue samples under static or slow loading conditions and may vary from those under high speed loading. Other failure thresholds, such as strain and elongation, can be found in the literature report (Webber, Niu et al. 2017). Occurrence of tissue failure from high strain-rate deformation was not available.

Table 4-4. Summary of failure stress of vertebrae, disc and facet joint.

Tissue	Failure Indicator	Failure Values	Reference
Vertebrae Cortical Bone	VM-Stress (MPa)	112.7 (92~161)	Reilly and Burstein (1975), Zhao and Narwani (2007)
Vertebrae Trabecular Bone	VM-Stress (MPa)	4.8 (3.14~10.1)	Yamada (1970), Zhao and Narwani (2007)
Disc Annulus	VM-Stress (MPa)	7.55±4.85	Yoganandan, Kumaresan et al. (2001)
Facet Joint	VM-Stress (MPa)	5.67±1.47	Yoganandan, Kumaresan et al. (2001)

4.1.2 Data Validation Task Analysis

The detailed of PMHS impact tests is given in corresponding report (Mathews and Webber 2017). It included the data correction and validation of accelerometer measurement with high-speed video. The general following steps were conducted to validate the accelerometer measurements:

- The impact speed measured from high speed video as first standard;
- The measured flight distances from projectile header to target as second standard;
- Identify the time of blunt impact on target;
- Correct the drifting using the measurement begin projectile accelerate;
- Integrate acceleration once to get maximum speed;
- Integrate acceleration twice to get flight distances;
- Comparing the impact speeds from video and acceleration, flight distances from measurement and acceleration to correct the sensor calibration factor;
- Validate the calibration factors by calculate the bear length from accelerometer measurement;

4.1.3 Required Validation Data

No data was required to validate at this section.

4.2 Conceptual Model Validation Tasks Analysis

Several activities are performed to validate the conceptual models in use by this M&S. The geometric, FE meshing, and material model accuracy of the FE representation of the torso organs can be determined by standard model checks. Many of the FEM's concept validation activities shall be performed on each organ individually, while others will be conducted upon the FEM as a whole.

- **Anatomical Accuracy:** Proof of which is obtained by comparing area or volume to the values found in the raw source geometry. This test satisfies requirement 3.1.1.1.
- **Mesh Quality:** Several statistics are available to quantify mesh quality, such as minimum angle and element Jacobians. This test satisfies requirement 3.1.1.2.
- **Material Models:** The applied material models can be evaluated according to how closely they can reproduce test data and the maximum loading rate for which the material model is stable. This test satisfies requirement 3.1.1.3.
- **Parameter Sensitivity:** Because the material properties will vary due to large differences in typical human tissue samples, response sensitivity to material property perturbations should be studied to ensure the output does not vary disproportionately to small changes in input properties. A secondary benefit will be that the output parameters that vary least are likely to be the best predictors of injury. This test satisfies requirement 3.1.2.4.
- **Simulation Stability & Energy Convergence:** The simulation of model should be stable under reasonable threat and computational cost should be efficient. The energy should be convergent enough to keep accurate results. This test satisfies requirement 3.1.2.5 and 3.1.2.6.

4.2.1 Anatomical Accuracy

The organ anatomy was extracted from Zygote 3D Male Human Model and the geometry was accurate enough to construct human torso organs in the FE model using HyperMesh. Figure 4-8 gives the mesh of ribcage (spine, ribs, costal-cartilages, sternum), internal organs (lungs, liver, spleen, stomach, kidneys), and body exterior tissue. In this model, the spine includes the vertebrae (C5-L5), discs, and facet joints. The shoulder includes scapula, clavicle and humerus. Table 4-5 lists the total number of nodes, elements and parts.

Table 4-5. Nodes, elements and parts of human torso FEM.

Nodes	Total	1,269,774
Element	Total	6,971,258
	Tetra4	6,765,273
	Tria3	201,346
	Beam	3,222
	Spring	1,417
Part	Total	129

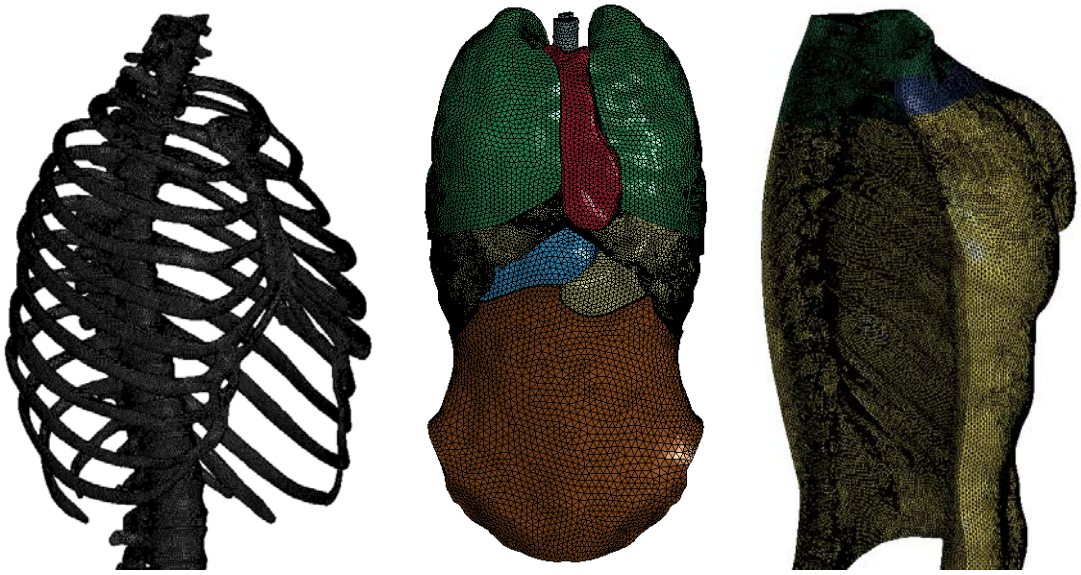

Ribcage Internal Organs Body Exterior Tissue

Figure 4-8. Meshes of human torso model.

Small gaps exist when the tissue and fat between chest wall and internal organs are disregarded. For example, there are gaps between ribs and lung when their anatomical geometries are put together, shown in Figure 4-9. To reduce or eliminate these gaps, the outside lung surface is adjusted to lay close to the internal ribcage surface during the mesh construction. For the purpose of simulation stability (e.g., minimizing contact interfaces), mesh continuity is maintained between vertebrae and disc, bones (ribs, costal-cartilages, sternum, shoulder bones) and exterior tissue (muscle/skin). Figure 4-10 shows the mesh of vertebrae and disc, bones and exterior tissue. The vertebrae connected disc and the bones buried inside muscle, where nodes are shared in their connections.

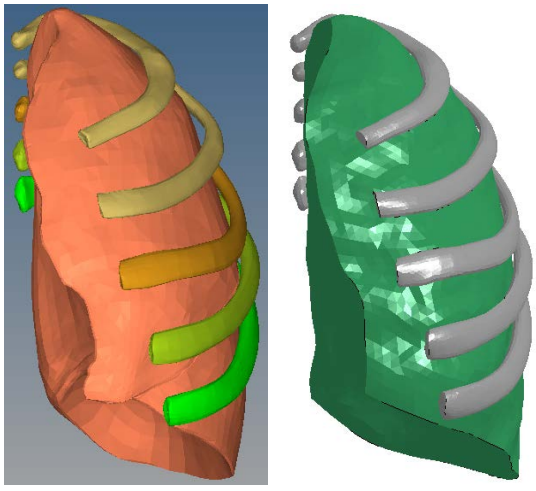

Anatomy Mesh

Figure 4-9. Anatomy and mesh of lung and ribs

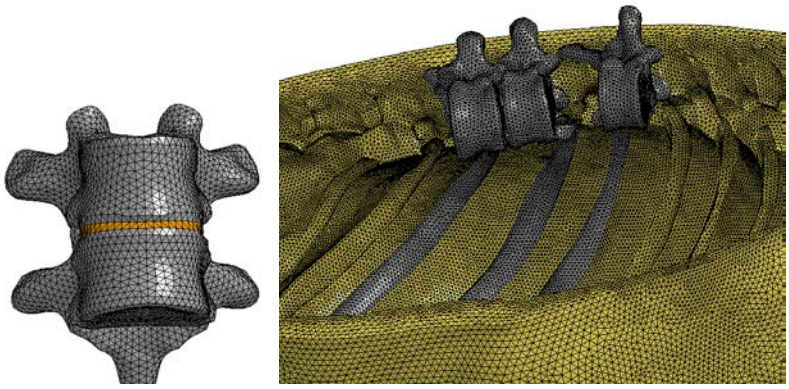

Figure 4-10. Mesh continuity of spine, bones and muscle.

The comparison of surfaces and volume of torso organs from model and anatomy is given in Table 4-6. The maximum variations of surface and volume for ribs, costal-cartilages, sternum, and vertebrae were less 3%. The maximum of surface difference for lungs and kidneys was 5.0%, while the variations between model and anatomy for liver, spleen and stomach were 19.2, 52.5% and 25.6%, respectively. The biggest variations were caused by projection of surfaces of these organs to the internal chest wall surface to remove gaps. Zygote's geometry showed gaps that were perhaps a result of fat or other tissue that were not accounted for or due to the anatomical inaccuracy of original source. For example, see Figure 4-11 which compares the original Zygote anatomy with the constructed model of spleen in the current FE model. Large gaps between spleen and chest wall are apparent in original anatomy. To reduce the gap, the spleen surface was offset to the chest wall and the spleen artificially increased in size.

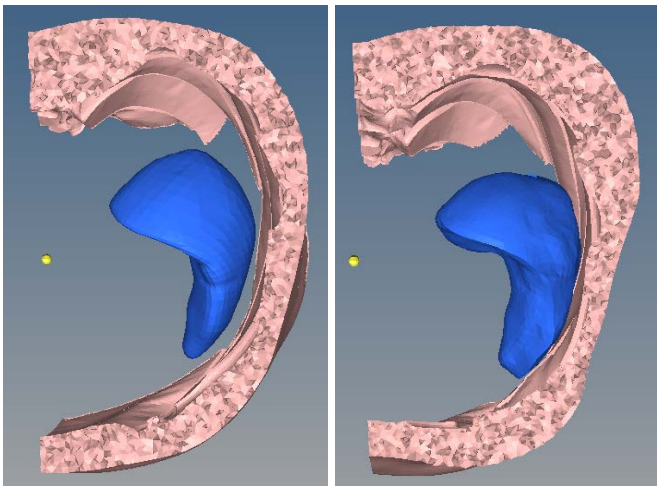

Figure 4-11. Anatomy and model of spleen.

Table 4-6. Geometry Comparison Between Anatomy and Mesh.

Part Name	Surface (mm^2)			Volume (mm^3)		
	Anatomy	**Mesh**	**Variation %**	**Anatomy**	**Mesh**	**Variation %**
Rib01	4566.1	4464.8	2.2	8431.7	8185.3	2.9
Rib02	6989.8	6873.4	1.7	14800.2	14454.7	2.3
Rib03	8782.9	8639.1	1.6	17224.4	16774.1	2.6
Rib04	10864.2	10669.5	1.8	24478.8	23944.8	2.2
Rib05	12048.4	11887.8	1.3	30049.2	29577.3	1.6
Rib06	13008.6	12820.9	1.4	33558.7	32997.9	1.7
Rib07	12404.1	12249.9	1.2	31626.9	31103.8	1.7
Rib08	11512.1	11440.5	0.6	26728.6	26626.6	0.4
Rib09	10754.2	10648.9	1.0	24744.6	24518.3	0.9
Rib10	9064.7	8917.1	1.6	19119.0	18639.4	2.5
Rib11	6143.3	6085.8	0.9	12788.3	12624.5	1.3
Rib12	2792.2	2740.7	1.8	5040.0	4902.1	2.7
CostalCartilage01	1255.2	1242.9	1.0	3080.6	3065.3	0.5
CostalCartilage02	1546.8	1549.4	0.2	3113.7	3065.0	1.6
CostalCartilage03	1887.2	1871.1	0.9	4299.3	4241.4	1.3
CostalCartilage04	2067.2	2080.0	0.6	4708.4	4649.0	1.3
CostalCartilage05	2798.8	2772.0	1.0	6568.4	6463.7	1.6
CostalCartilage06	13613.5	13618.1	0.0	29488.2	29258.4	0.8
Sternum	13563.3	13665.7	0.8	50437.1	51004.5	1.1
C5	4630.9	4500.7	2.8	9747.6	9476.6	2.8
C6	5122.9	5074.6	0.9	11423.0	11120.3	2.6
C7	6084.0	5909.1	2.9	14592.2	14262.1	2.3
T1	7089.8	7014.9	1.1	23526.8	23272.2	1.1
T2	7137.3	7077.4	0.8	24608.1	24405.2	0.8
T3	7284.6	7229.6	0.8	24690.9	24492.3	0.8
T4	7640.4	7521.8	1.6	25928.9	25670.5	1.0
T5	7687.1	7591.0	1.2	26086.0	25843.0	0.9
T6	8322.2	8234.0	1.1	29616.2	29328.8	1.0
T7	8576.6	8488.0	1.0	32157.5	31923.9	0.7
T8	8765.8	8666.8	1.1	33971.4	33754.2	0.6
T9	9077.6	8992.9	0.9	35637.2	35436.5	0.6
T10	9582.9	9457.5	1.3	39290.4	39088.7	0.5
T11	10090.8	9968.7	1.2	44100.5	43754.6	0.8
T12	10776.1	10643.4	1.2	50005.3	49689.5	0.6
L1	11947.4	11785.6	1.4	54465.0	54045.6	0.8
L2	12969.2	12759.2	1.6	57566.7	57035.8	0.9
L3	13618.4	13446.3	1.3	59252.7	58958.9	0.5
L4	13600.2	13452.4	1.1	62239.1	61901.3	0.5

L5	12542.6	12392.0	1.2	55792.9	55451.3	0.6
Left Lung	120861.0	118060.0	2.3			
Right Lung	128415.3	121951.0	5.0			
Liver	60954.5	72661.1	19.2			
Spleen	60954.5	28953.6	52.5			
Stomach	27595.9	34649.8	25.6			
Left Kidney	12832.3	12637.8	1.5			
Right Kidney	13131.8	12906.5	1.7			

4.2.2 Mesh Quality

Table 4-7 contains a summary of the mesh quality statistics. The good ranges given in Table 4-7 reflect the optimized values in HyperMesh that were recommended to achieve the best computational efficiency. In this human torso FEM, only a small percentage of elements failed in checks the of collapse, skew, aspect ratio, and trial face angle. Additionally, the reported worst values of the mesh were far from the failure thresholds, thus the torso FEM has a stable and efficient mesh, which is demonstrated in a later study.

Table 4-7. Mesh quality statistics of human torso FEM.

Quality	Ideal	Good value	No. of failed good range	Failed % of good vale	Model worst value	Failure threshold
Tet collapse	1	>0.4	284	0.004%	0.31	0
Vol Skew	0	<0.6	28,096	0.415%	0.80	1
Aspect Ratio	1	1-4	0	0.000%	3.32	12
Skew	0	0-50	1,075	0.016%	58.7	90
Cell squish	0	0-0.5	1,002	0.015%	0.64	1
Tria face min angle	60	>20	152	0.001%	18.0	0
Tria face max angle	60	<120	16	0.001%	122.9	180

4.2.3 Material Models for Torso Organs

The summary of the material models in the human torso FEM is given in Table 4-8. The rib is modelled as two typical parts, shell cortical and solid trabecular, where the thickness of cortical was assumed to be uniformly 1mm (Li, Kindig et al. 2010). The values of rib cortical modulus were reported as 6.2~10.1GPa (Kimpara 2015), 9.2~10.2GPa (Stein and Granik 1976), 11.5GPa (Granik and Stein 1973), 7.5~11.9GPa (Stitzel, Cormier et al. 2003), from three-point bending tests, 13.3~15.1GPa (Kemper, McNally et al. 2007), 13.9GPa (Kemper, McNally et al. 2005), 11.4~18.5GPa (Subit, de Dios et al. 2011) from couple tension tests, 18.9~21.1GPa (Kemper,

McNally et al. 2007) from whole rib bending tests, and 7.1±2.5GPa and 11.6±1.9GPa for child and adult (Zhu, Bermond et al. 2017). The modulus of rib cortical is assigned to be 10GPa which falls within the mean values from literature. Similar values were also used in other FE models, i.e., 11.5GPa by Li, Kindig et al. (2010), 9.86GPa in THMUS (Shigeta, Kitagawa et al. 2009), 10.8GPa in TKHM (Zhao and Narwani 2005), and 9~15GPa in HUMOS (Arnoux, Serre et al. 2008). The value of rib trabecular modulus is 40MPa, which is in the range of reported values from literature. Rib costal-cartilage is assumed to be elastic with a modulus of 450MPa (Arnoux, Serre et al. 2008). Sternum is assumed to be homogenous elastic with a 5GPa Young's modulus.

Table 4-8. Material models used in human torso FEM.

Organ	**Material Model**	**Reference**
Rib Cortical	D=1800 kg/m^3; Elastic E= 10 GPa, v=0.3	Kimpara (2015), Stitzel, Cormier et al. (2003)
Rib Trabecular	D=1400 kg/m^3; Elastic E= 40 MPa, v=0.3	Li, Kindig et al. (2010), Shigeta, Kitagawa et al. (2009)
Rib Costal-Cartilage	D=1200 kg/m^3; Elastic E= 500 MPa, v=0.3	Arnoux, Serre et al. (2008)
Sternum	D=1600 kg/m^3; Elastic E= 5 GPa, v=0.3	Simplified elastic
Vertebral Trabecular	D=1000 kg/m^3; Elastic E= 100 MPa, v=0.35	Kumaresan, Yoganandan et al. (1999)
Vertebral Cortical	D=2000 kg/m^3; Elastic E=8 GPa, v=0.3	Zhao and Narwani (2007), Noailly, Ambrosio et al. (2012)
Disc Nucleus	D=1000 kg/m^3; Elastic E=8 MPa, v=0.45	Ben-Hatira, Saidane et al. (2012)
Disc Annulus	D=1000 kg/m^3; Elastic E=100 MPa, v=0.3	Meyer, Bourdet et al. (2004)
Scapula, Clavicle, Humerus	D=1800 kg/m^3; Elastic E=10 GPa, v=0.3	Ben-Hatira, Saidane et al. (2012)
Lungs	Hydro dynamic, G=733Pa, EOS: C1=100kPa, C2=800kPa	Shen and Niu (2008)
Bronchial & Esophagus interior	Elastic fluid (D=11 kg/m^3; K= 11 MPa)	Trachea and esophagus filled with 1% water, 99% air
Lung Pleura	Viscoelastic, K=10MPa, G1=3MPa, Beta1=1000	Shen and Niu (2008)
Bronchial Tress Cartilage	D=1000 kg/m^3; Elastic E=17 MPa, v=0.45	Safshekan, Tafazzoli-Shadpour et al. (2016)
Diaphragm	D=1000 kg/m^3; Elastic E=100 MPa, v=0.3	Shen and Niu (2008)

Liver	Ogden rubber (Mu1=G1=25KPa, Alfa1=8.8, G2=3MPa, Beta1=0.01, Beta2=10000)	Mean curve
Spleen	Ogden rubber (Mu1=G1=15KPa, Alfa1=7.4, G2=2MPa, Beta1=0.01, Beta2=10000)	Mean Curve
Stomach & intestine interior	Ogden rubber (Mu1=G1=5.5KPa, Alfa1=9.8, G2=1MPa, Beta1=0.001, Beta2=20000)	Filling soft muscle
Pancreas	Hyperelastic rubber	Song, Chen et al. (2007)
Stomach, intestine	D=1000 kg/m^3; Elastic E=687 kPa, v=0.45	
Esophagus	D=1000 kg/m^3; Hyperelastic rubber	Yamada (1970)
Heart	D=1000 kg/m^3; Elastic E=3 MPa, v=0.45	Simple elastic
Vessel Blood	Elastic fluid (D=1000 kg/m^3; K=1.1 GPa, reduce to increase time step)	Filled with water
Vessel Tissue	D=1000 kg/m^3; Elastic E=9.98 MPa, v=0.45	Karimi, Navidbakhsh et al. (2014)
Kidneys	Ogden rubber (Mu1=G1=30KPa, Alfa1=10, G2=2MPa, Beta1=0.001, Beta2=20000)	Mean curve
Connections among clavicle, sternum, scapula, ribs, spine	D=1200 kg/m^3; Elastic E=450 MPa, v=0.45	Use cartilage
Facet Joints	D=1000 kg/m^3; Elastic E=10 MPa, v=0.45	Halldin, Brolin et al. (2000), Hedenstierna (2008)
Ligament	Tension-only spring	(Kumaresan, Yoganandan et al. 1999)
Muscle/Skin Tissue	Ogden rubber (Mu1=G1=30KPa, Alfa1=9.8, G2=4MPa, Beta1=0.001, Beta2=20000)	Mean curve

The engineering stress-strain curves of muscle, liver, spleen, kidney, stomach and intestine are given in Figure 4-12 to Figure 4-16, respectively. The Ogden rubber model is used to simulate the soft organs material property, and current model approximately represents the mean among all curves. The material properties are obtained from literature test data and models and then converted into stress-strain curves by formulation manipulation or compression simulations.

The muscle curves come from tests (Yamada 1970), (Vannah and Childress 1996), (Song, Chen et al. 2007), (Chawla, Mukherjee et al. 2009), and models (Lizee, Robin et al. 1998), (Meyer, Bourdet et al. 2004), (Zhao and Narwani 2005), (Roberts, Merkle et al. 2007), (Arnoux, Serre et al. 2008), (Shigeta, Kitagawa et al. 2009), respectively.

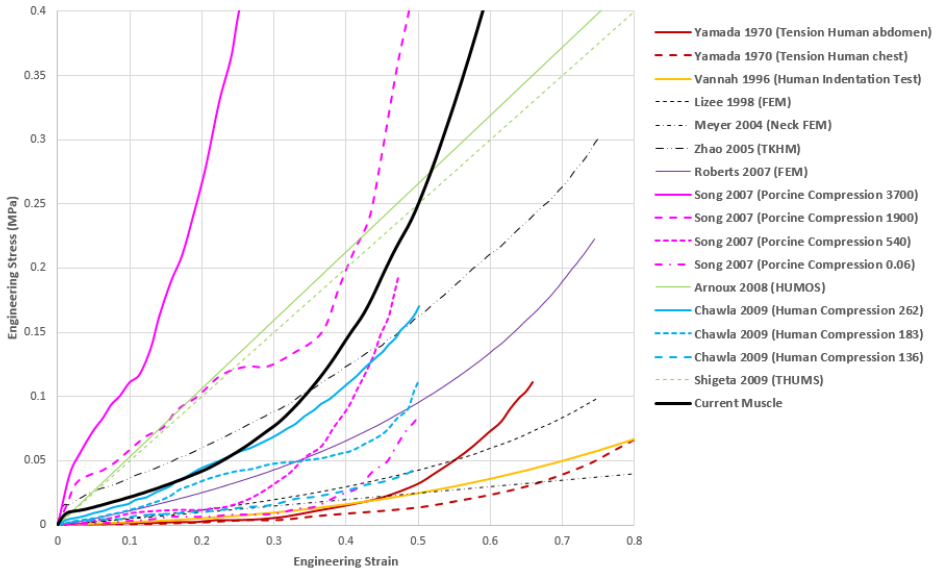

Figure 4-12. Engineering stress-strain curves of muscle.

The liver curves come from tests (Umale, Deck et al. 2012), (Kemper, Santago et al. 2011), (Gao, Lister et al. 2010), (Rosen, Brown et al. 2008), (Sparks 2007), (Tamura, Omori et al. 2002) and models (Shigeta, Kitagawa et al. 2009), (Arnoux, Serre et al. 2008), (Roberts, Merkle et al. 2007).

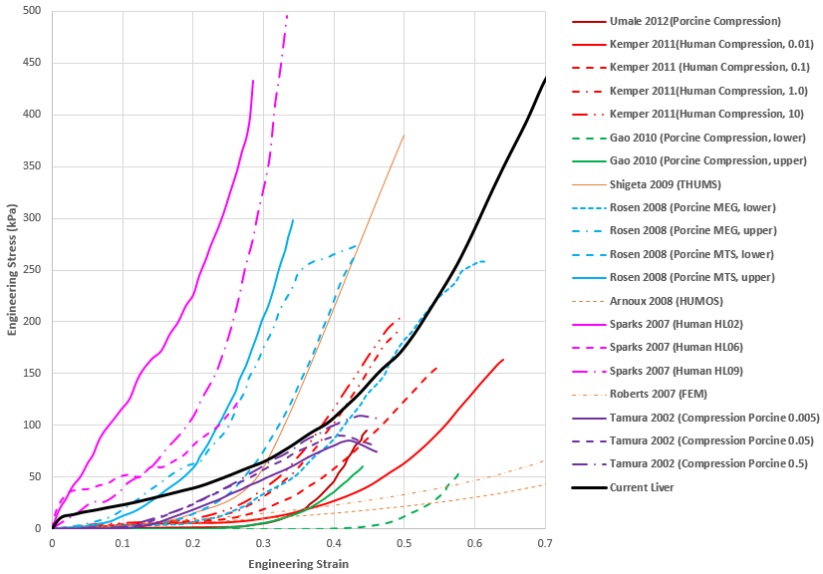

Figure 4-13. Engineering stress-strain curves of liver.

The spleen material curves come from tests (Umale, Deck et al. 2012), (Kemper, Santago et al. 2012), (Kemper, Santago et al. 2011), (Rosen, Brown et al. 2008), (Tamura, Omori et al. 2002), (Carter, Frank et al. 2001) and models (Shigeta, Kitagawa et al. 2009), (Zhao and Narwani 2005), (Arnoux, Serre et al. 2008), respectively.

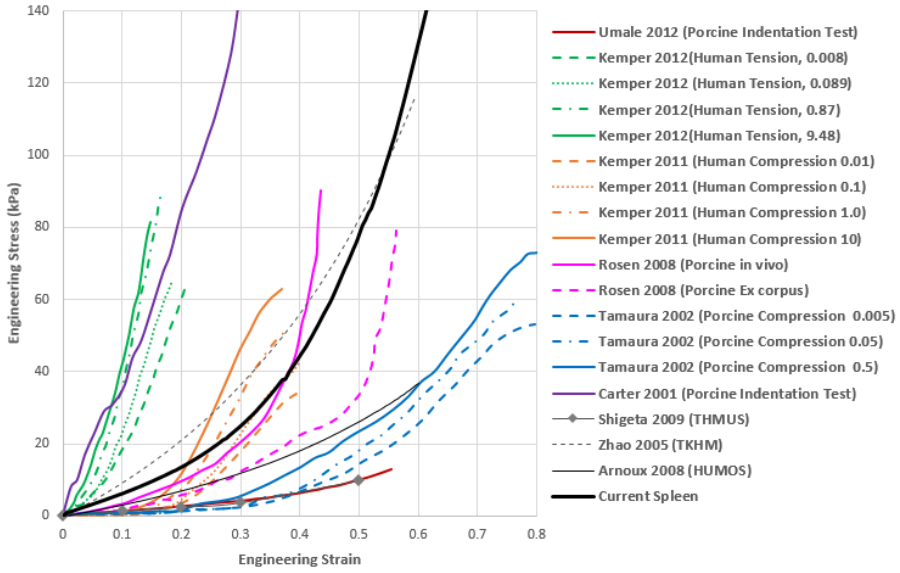

Figure 4-14. Engineering stress-strain curves of spleen.

The stress-strain curves for kidney were extracted from tests (Umale, Deck et al. 2012), (Snedeker, Barbezat et al. 2005), (Tamura, Omori et al. 2002), (Farshad, Barbezat et al. 1999) and models (Shigeta, Kitagawa et al. 2009), (Arnoux, Serre et al. 2008).

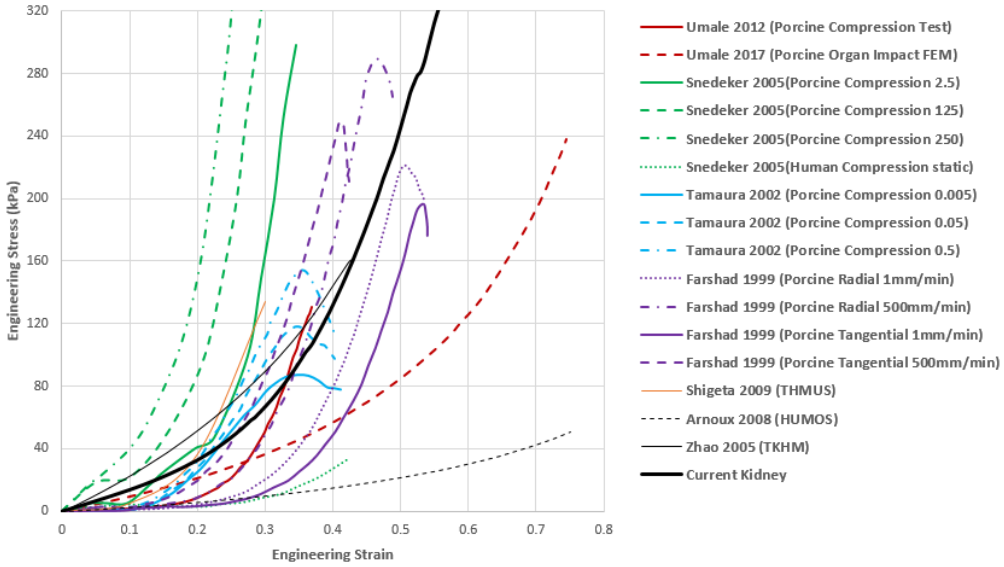

Figure 4-15. Engineering stress-strain curves of kidney.

The stress-strain curves of intestine and stomach were extracted from tests (Rosen, Brown et al. 2008), (Egorov, Schastlivtsev et al. 2002) and models (Shigeta, Kitagawa et al. 2009), (Arnoux, Serre et al. 2008), (Zhao and Narwani 2005). The intestine and stomach are modeled with the tissue represented as a shell and the fluid represented as a solid. For model simplicity and stability, the tissue material is assumed to be elastic and the mean modulus as 687kPa in the higher strain region (strain >0.2).

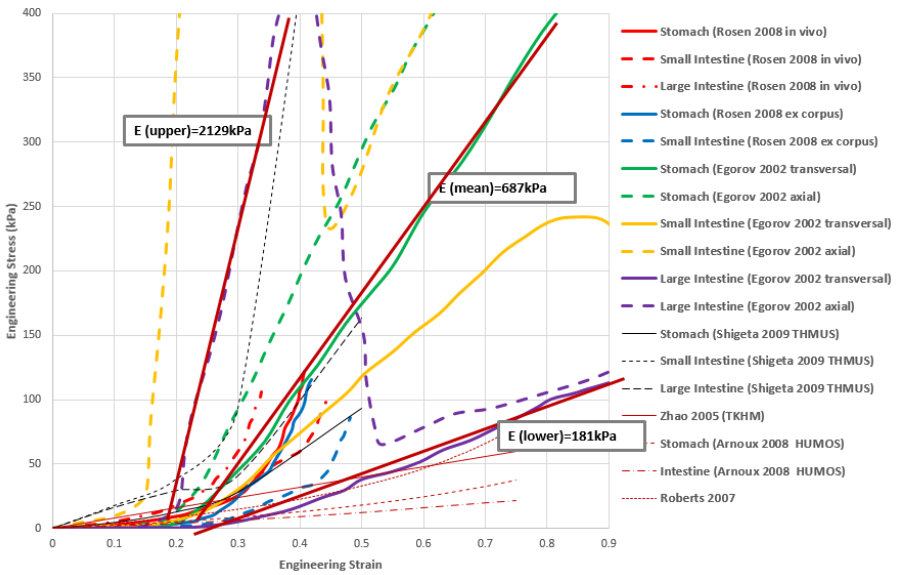

Figure 4-16. Engineering stress-strain curves of intestine & stomach.

4.3 Design Verification Task Analysis

This subsection describes the analysis of the results of each design verification task.

The design of the M&S is verified through a series of checks intended to identify and remedy any improper numerical artifacts within the FEM. Furthermore, each task verifies that two or more aspects of the model are interacting together properly. These tasks are:

- **Uncertainty & Sensitivity:** Because the material properties will vary due to large differences in typical human tissue samples, response sensitivity to material property perturbations should be studied to ensure the output does not vary disproportionately to small changes in input properties. A secondary benefit will be that the output parameters that vary least are likely to be the best predictors of injury. This test satisfies requirement 3.1.2.4.
- **Mesh Convergence:** An appropriate level of mesh discretization must be determined to ensure that the FEM is capturing the phenomena that is intended by the model. The simulation results from three meshes with different densities must be compared to identify the appropriate element size to achieve converged results. This test satisfies requirement 3.1.1.2.
- **Computational Stability:** It is fundamental that the model can fully complete the simulations under general loading conditions. This study is to check the model stability under extreme loading, such as projectiles with large mass and high speed, which causes large deformation. It also provides a check of model initialization, energy convergence and limitations.

4.3.1 Uncertainty Study of Material Models in FEM

The material properties show extensive variations from literature data. The engineering stress-strain curves of muscle, liver, spleen, kidney and intestine & stomach are plotted in Figure 4-12 to Figure 4-16, respectively. An uncertainty study was conducted on the material variations of body exterior tissue (muscle/skin), ribs, lungs, liver, stomach and intestine by simulation blunt impact on swine FE model. The material model of ribs is elastic, where the Young's modulus falls within the range of 6~14GPa. The lung is modeled as an elastic plastic hydro dynamic model, where EOS (equation of state) is used to control pressure-volumetric behavior. Material variation was accomplished by adjusting the values of parameter C1 (30~500kPa). The intestine and stomach were simplified as elastic with its modulus in the range of 181~2129kPa. Ogden rubber model is used to simulate the material properties of body exterior tissue and liver. To generate varied material models fitting the stress-strain curves from literatures, the following two steps were implemented. First, calibrated models (soft, base, and hard) were generated using inverse FE technology. The method allows for adjustment to parameter values of Ogden material models during simulated compression until the stress-strain curve replicates the desired stress-strain curve as shown in Figure 4-17. The second step is to generate the intermediate stress-strain models by interpolating the parameters of calibrated models. The stress-strain curves of intermediate models shown in Figure 4-18 fall within those of the calibrated models. The study of material uncertainty is detailed in a separated technical report.

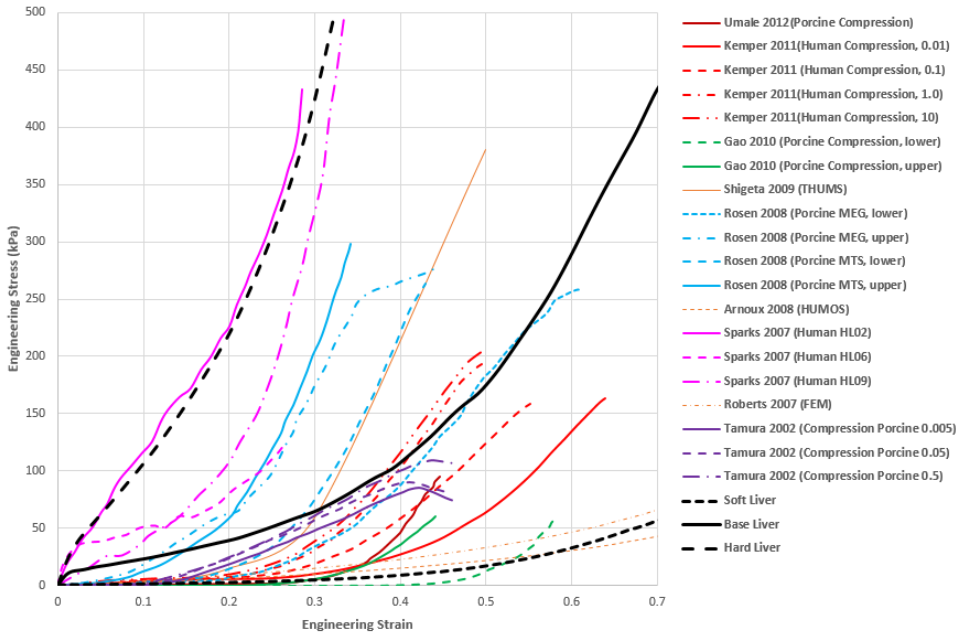

Figure 4-17. Stress-strain curves from literature data and calibrated models (soft, base, hard).

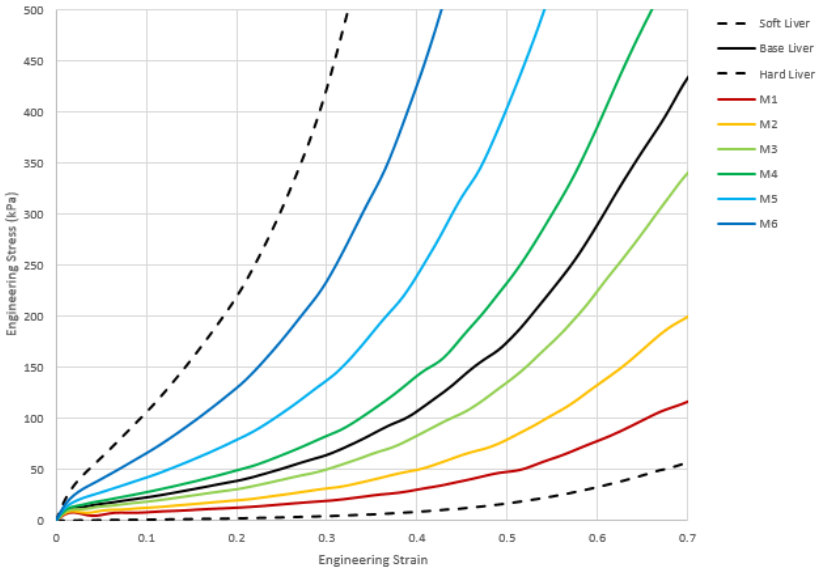

Figure 4-18. Stress-strain curves of calibrated (soft, base, hard) and intermediate models.

4.3.2 Mesh Convergence Study of FEM

The mesh convergence study is designed find the desired mesh resolutions by balancing simulation accuracy with the computational cost and time of an overly fine mesh. Study of mesh sensitivity was conducted on rib, liver and lung. The rib is considered a hard material with a cortical modulus of the order of GPa's. The liver is a soft organ with an overall modulus of the order of kPa to MPa. The lung is the softest organ with a density that is 10~40% of water and the remainder behaving as a gas/fluid in vivo.

Three meshes of left rib#6 were constructed and the mesh configurations are given in Table 4-9. The rib was impacted by a rigid projectile on the exterior side with the simulation setup shown in Figure 4-19. The rib was fixed at both ends and covered by 8mm thickness tissue which mesh resolution (1mm) for each of the three rib meshes. The simulation used a 25mm diameter cylindrical projectile that weighed 50gram with an impact speed of 30m/s. The contact force history of three rib meshes is plotted in Figure 4-20. Peak mechanical response, including peak contact forces, and rib stress and strain under impact location are listed in Table 4-10. The variations of stress and strain between Mesh1 (1mm element) and Mesh2 (2mm element) are both less than 2%, thus the 2mm element size is sufficient for simulation accuracy. Increasing mesh fineness (Mesh2 to Mesh1) will result in very high computational cost with little improvement to accuracy.

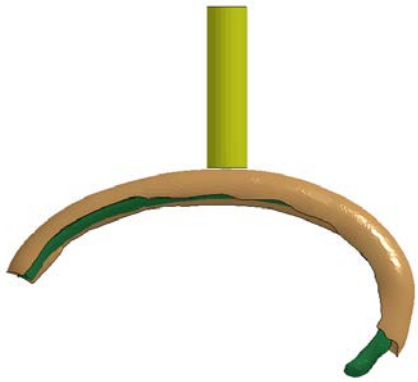

Figure 4-19. Rib impact simulations for mesh convergence study.

Table 4-9. Three meshes of left rib#6 for mesh convergence study.

	Mesh1	Mesh2	Mesh3
Element size (mm)	1	2	3
Nodes	16,758	5,573	2.498
Elements	79,612	22,237	9,556

Table 4-10. Peak mechanical responses of rib impact for mesh sensitivity study.

Element size (mm)	1mm	2mm	3mm	Diff. Mesh1~2	Diff. Mesh2~3
Peak Contact Force (kN)	2.59	2.49	2.35	3.86%	5.62%
Non Mises Stress (MPa)	179.1	176.1	170.6	1.68%	3.12%
1st principal Stress (MPa)	187.1	184	182	1.66%	1.09%
1st principal Strain (%)	1.84	1.82	1.76	1.09%	3.30%

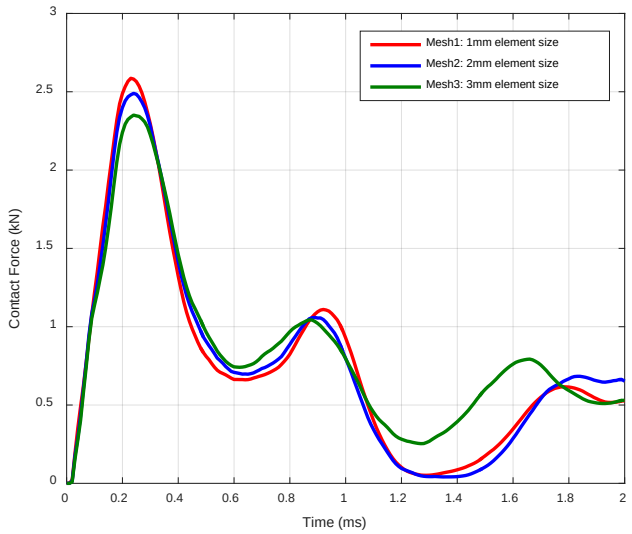

Figure 4-20. Contact force history of rib impact for mesh sensitivity study.

Three meshes of the liver were used to study the mesh convergence of soft organs. The element size, number of node and elements of three meshes are listed in Table 4-11. A rigid umbrella shaped impactor weighing 50 grams at a speed of 30 m/s was used to simulate an impact to the upper region of the liver (Figure 4-21). The contact force history from three meshes plotted in Figure 4-22 were almost identical. The peaks of contact forces, liver internal energy, stress (von Mises and principal) and volume percentages of lacerated (principal stress > 189kPa) are given in Table 4-12. The differences of stress between Mesh1 (3mm element) and Mesh2 (5mm element) are less than 4%. Considering the simulation time, the 5mm element size is sufficient to construct soft organs with convergent results.

Table 4-11. Three meshes of liver for mesh convergence study.

	Mesh1	Mesh2	Mesh3
Element size (mm)	3	5	7
Nodes	111,165	25,960	7,463
Elements	634,660	144.714	39,525

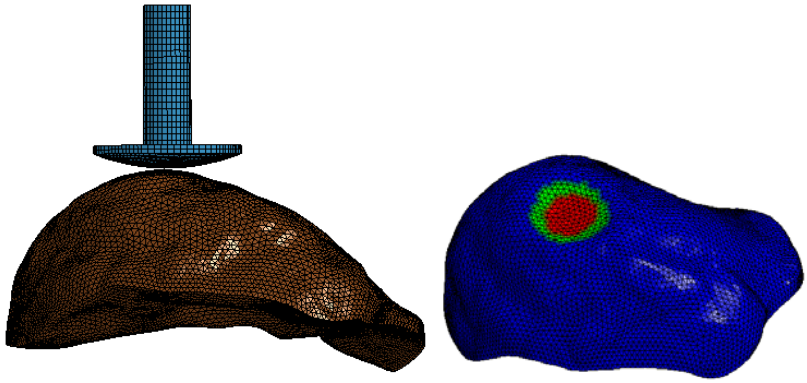

Figure 4-21. Live impact simulation for mesh sensitivity study.

Table 4-12. Peak mechanical response of liver impact for mesh convergence study.

Element size (mm)	3mm	5mm	7mm	Diff. Mesh1~2	Diff. Mesh 2~3
Peak Force (kN)	2.91	2.9	2.84	0.34%	2.07%
Internal Energy (J)	21	20.9	20.6	0.48%	1.44%
VM Stress (KPa)	961.9	954.2	896.1	0.80%	6.09%
1st PR Stress (MPa)	1.71	1.65	1.55	3.51%	6.06%

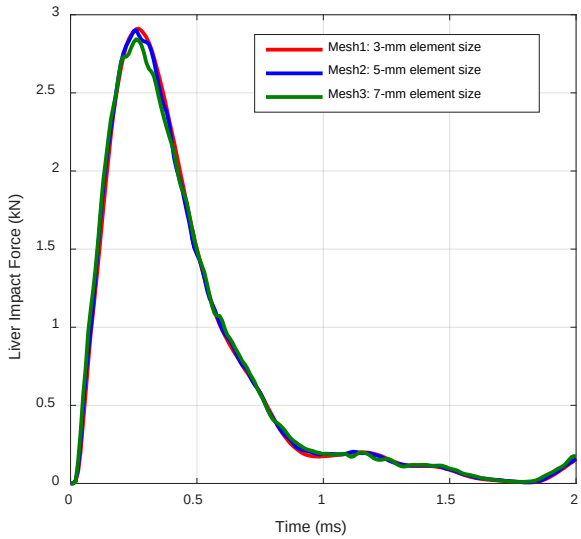

Figure 4-22. Contact forces of liver impact for mesh sensitivity study.

For the lung, the same 3, 5, 7mm element sizes are tested (Table 4-13). Impacts from a rigid, mushroom shaped projectile weighing 50 grams at a speed of 20 m/s were simulated to the side of the lung. The simulation setup is shown in Figure 4-23. The simulation results given in Table 4-14 include delivered energy (internal energy of lung), peak pressure at impact location and the percentages of contused volume. The contused percentage was the volume of contused elements (strain energy density > 3.5kPa) divided the whole lung. The contact force history and the volume percentages are plotted at Figure 4-24, where the volume percentage (y-axis) means the volume percentage of elements whose strain energy density is larger than the threshold (x-axis). It can be seen that differences of the peak pressure and contused percentages between Mesh1 (3mm element) and Mesh2 (5mm element) are both less 2%, and the contact forces and volume percentage distribution are both convergent. It can be concluded the 5mm element size is a sufficient resolution for lung impact simulations.

Table 4-13. Three meshes of lung for mesh sensitivity study.

	Mesh1	Mesh2	Mesh3
Element size (mm)	3	5	7
Nodes	150,001	49,637	18,843
Elements	852,243	279,296	103,573

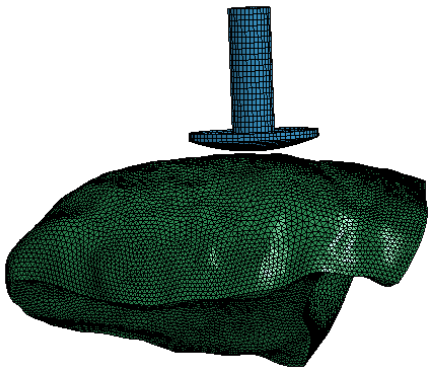

Figure 4-23. Lung impact simulations for mesh sensitivity study.

Table 4-14. Simulation results of lung impacts for mesh sensitivity study.

Element size (mm)	3mm	5mm	7mm	Diff Mesh1~2	Diff Mesh2~3
Internal Energy (J)	3.57	3.53	3.43	1.12%	2.83%
Peak Pressure (kPa)	208.5	205.9	196.5	1.25%	4.57%
Contusion Percentage (%)	30.7	30.2	28.8	1.63%	4.64%

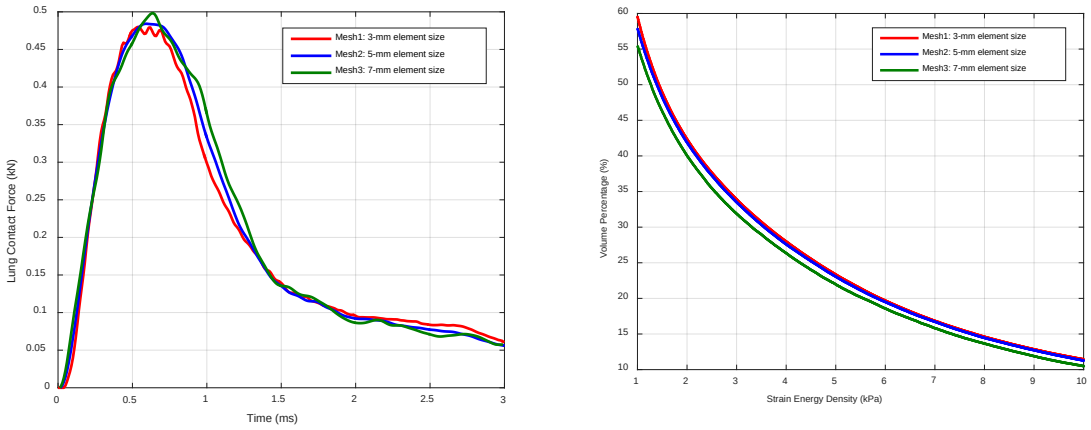

Figure 4-24. Contact forces and volume percentages vs. strain energy density of lung impact.

4.3.3 Computational Stability Study

A blunt impact simulation with extreme loading was conducted to study computational stability, model initialization, and energy convergence. The simulation setup is shown in Figure 4-25. The 6-inch diameter cylinder pendulum impactor weighing 23.4 kilograms and impacting the chest (sternum) at speed 40m/s is simulated. The 3-ms simulation was conducted and completed within 16 hours with no failure of elements. The penetrations among contact interfaces were very small

(<0.5mm, see Section 4.4.1) so the penetrations didn't need to be removed for model initialization. Thus, the initial internal energy is zero. The FE model shows the ability to handle large deformation even for very severe body compressions, as shown in Figure 4-26. The meshing methodology implemented in torso FE will not cause hourglass energy, thus the energy is always convergent.

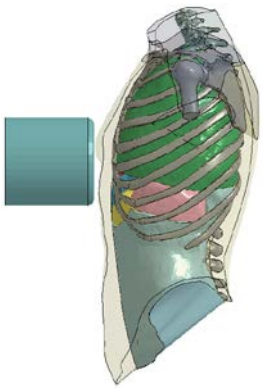

Figure 4-25. Simulation setup for model stability study.

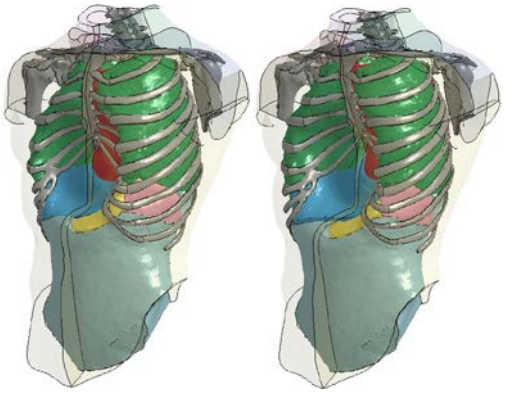

Figure 4-26. Severe compression occurs under large loading (t=2 ,3ms).

4.4 Implementation Verification Task Analysis

This subsection describes the analysis of the implementation verification test results. The overarching purpose of these tasks is to verify that the individual M&S components, such as material models, contact definitions, simulation parameters, geometry, and mesh, are incorporated into the M&S correctly.

4.4.1 Human Torso Model Assembly

In the torso model, the rib is modeled with 1-mm thickness shells for cortical bone and tetra solid for trabecular bone. The costal cartilages and sternum are modeled as homogenous solids. The ribs, costal cartilages and sternum are connected by shared nodes, as shown in Figure 4-27. In spine construction is shown in Figure 4-28, where the vertebrae are modeled as 1.5-mm

thickness shells for cortical bone and tetra solid elements for trabecular bone. The disc is meshed as solid elements connecting the endplates of vertebrae. The facet joint is simplified as beams to connect the corresponding vertebrae. Ligaments are simplified as a tension-only spring linking the two associated vertebrae. The beam elements are also used to connect the ribs to spine.

Figure 4-27. Models of rib, costal cartilage and sternum.

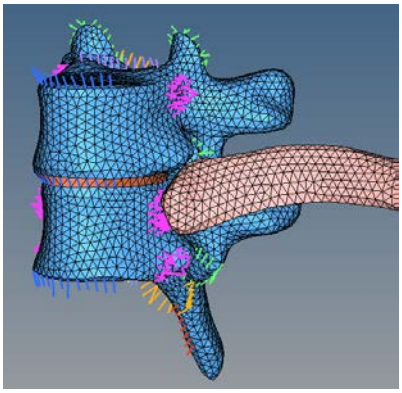

Figure 4-28. Models of spine (vertebrae, disc, facet joint, ligament), rib and connection

The gaps between internal organs and chest wall (ribcage and exterior tissue) are minimized by offsetting the organs surface to the interior surface of the chest wall. Lungs are meshed as solid elements and covered by lung pleura as shell elements. The heart is as treated as part of a bulk organ that includes the heart and surroundings tissues that occupy the space between the left and right lungs. Liver, spleen, and kidneys are modeled as homogenous solid elements. Stomach tissue is meshed as a shell and its interior as a solid. The lower region under the liver, spleen and stomach is considered to be the intestine, which is modeled with exterior shell elements and the interior as a fluid. The models of major internal organs are given in Figure 4-29. The gaps among organs were minimized by adjusting organs surfaces. The kidneys surrounded by lower abdomen tissue (intestine, hop muscle), are located below the liver and spleen, and does not directly contact the chest wall.

Figure 4-29. Models of internal organs in human torso FEM.

The assembled human torso FEM is shown in Figure 4-30. The chest wall consists of bone structures (ribcage and shoulder) and exterior body tissue. The bone structures include the ribcage and shoulder with shared nodes with exterior body tissue, thus the chest wall can be treated as one set when defining contacts. For the spine mesh, the vertebrae and disc are connected by shared nodes, thus no contacts need to be defined. The diaphragm is modeled as shell elements and connected to chest wall. Table 4-15 lists all contacts defined in the model. There are very few initial penetrations (<0.5mm) caused by different mesh on same surfaces between adjacent parts. All these contacts use automatic option and the segment-based constraint was adopted (SOFT=2). The static and dynamic friction factors were both set to 0.2. The erosion option was also implemented in the control time step card with ERODE=1.

Table 4-15. Contacts in human torso FEM.

Contact (ID Name)	Master ID (Part or Set)	Slave ID(Part or Set)	Penetration (mm)
(101)Chestwall-Diaphragm	Chestwall (8000)	Diaphragm (481007)	0.47
(201)Chestwall-RightLung	Chestwall (8000)	RightLung (481002)	0.02
(202)Chestwall-LeftLung	Chestwall (8000)	LeftLung (481001)	0.15
(203)Diaphragm-LeftLung	LeftLung (481001)	Diaphragm (481007)	0.45
(204)Diaphragm-RightLung	RightLung (481002)	Diaphragm (481007)	0.46
(301)Heart-Chestwall	Chestwall (8000)	Heart (485001)	0.00
(302)Heart-Diaphragm	Heart (485001)	Diaphragm (481007)	0.44
(303)Heart-LeftLung	LeftLung (481001)	Heart (485001)	0.03
(304)Heart-RightLung	RightLung (481002)	Heart (485001)	0.03
(401)Liver-Chestwall	Chestwall (8000)	Liver (482001)	0.00
(402)Liver-Diaphragm	Liver (482001)	Diaphragm (481007)	0.48
(501)Spleen-Chestwall	Chestwall (8000)	Spleen (483001)	0.00
(502)Spleen-Diaphragm	Spleen (483001)	Diaphragm (481007)	0.47
(601)Stomach-Chestwall	Chestwall (8000)	Stomach (484001)	0.01
(602)Stomach-Diaphragm	Stomach (484001)	Diaphragm (481007)	0.30
(603)Stomach-Liver	Liver (482001)	Stomach (484001)	0.03
(604)Stomach-Spleen	Spleen (483001)	Stomach (484001)	0.01

(701)Pancreas-Chestwall	Chestwall (8000)	Pancreas (484002)	0.00
(702)Pancreas-Liver	Liver (482001)	Pancreas (484002)	0.00
(702)Pancreas-Stomach	Stomach (484001)	Pancreas (484002)	0.00
(801)Chestwall-LeftKidney	Chestwall (8000)	LeftKidney (486002)	0.00
(802)Chestwall-RightKidney	Chestwall (8000)	RightKidney (486001)	0.00
(901)Intestine-Chestwall	Chestwall (8000)	Intestine (487001)	0.05
(902)Intestine-Liver	Intestine (487001)	Liver (482001)	0.27
(903)Intestine-Spleen	Intestine (487001)	Spleen (483001)	0.00
(904)Intestine-Stomach	Intestine (487001)	Stomach (484001)	0.00
(905)Intestine-Pancreas	Intestine (487001)	Pancreas (484002)	0.20
(906)Intestine-LeftKidney	Intestine (487001)	LeftKidney (486002)	0.00
(907)Intestine-RightKidney	Intestine (487001)	RightKidney (486001)	0.00
(908)Intestine-Diaphragm	Intestine (487001)	Diaphragm (481007)	0.49

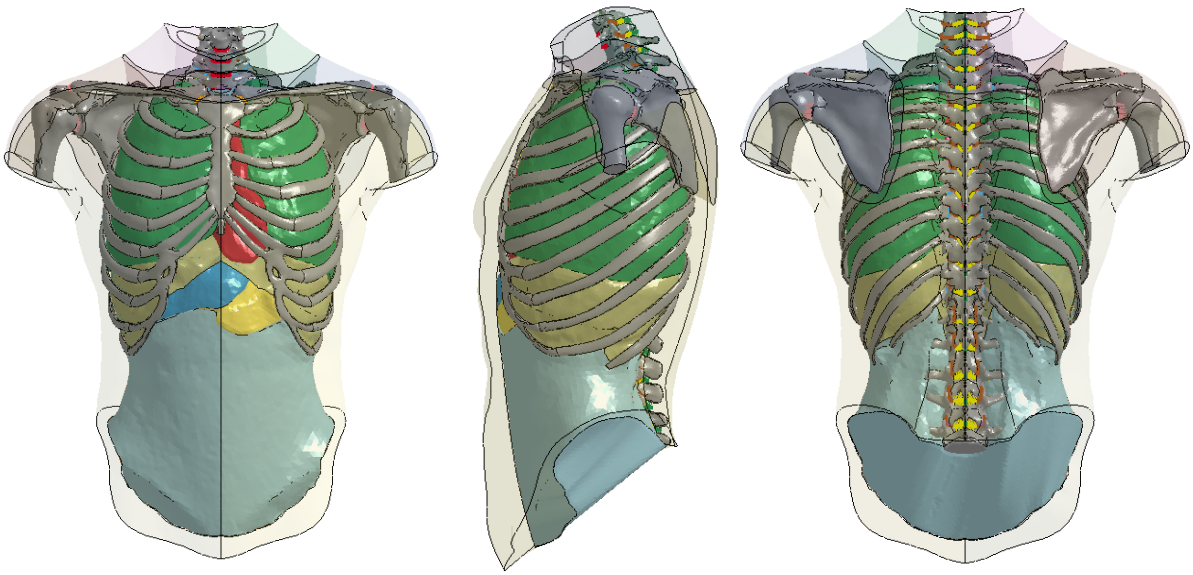

Figure 4-30. Human torso FEM (frontal, side and rear view).

4.5 Results Validation Task Analysis

This subsection describes the analysis of the validation test results. It correlates M&S results with acceptability criteria and M&S requirements as well as identifies the authoritative resources to be used in evaluating the M&S results.

4.5.1 Human Torso FEM Validation against MCW PMHS Impact Tests

The PMHS blunt impact tests conducted in 2017 (Mathews and Webber 2017) described at section 4.1.1.2 are used to validate the human torso model. Simulation configurations exactly follow test conditions. The model is scaled to match PMHS weight. The projectile is located at

the same location observed in tests and impact speed is same as measured in the test. Figure 4-31 shows examples of simulation setups for tests that aim at the intestine, stomach and kidney impacts, respectively. Three tests are simulated for each impact location. The comparisons of force history for impact on intestine, stomach, and kidney are plotted in Figure 4-32, Figure 4-33, Figure 4-34, respectively. The simulated forces overall match test measurements well. The simulated forces for intestine and stomach impacts are close to upper bound of tests data, while the simulated forces from kidney impacts fall inside the range of test measurements. As mentioned in previous section, the body exterior is modeled as a homogenous material model without consideration of composition differences between the front and back. However, the front exterior may have less muscle than back, which results in a lower stiffness than the back. Force comparisons of individual tests for each impact is shown in Figure 4-35. A very good match between test and simulation was found. All of these results demonstrate that the FE model produces accurate mechanical responses to relevant NLW impacts.

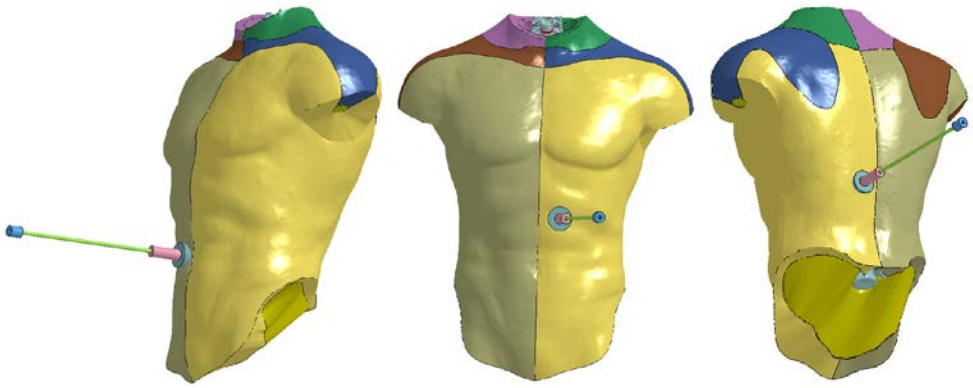

Figure 4-31. Simulations setups for PMHS intestine, stomach and kidney impact.

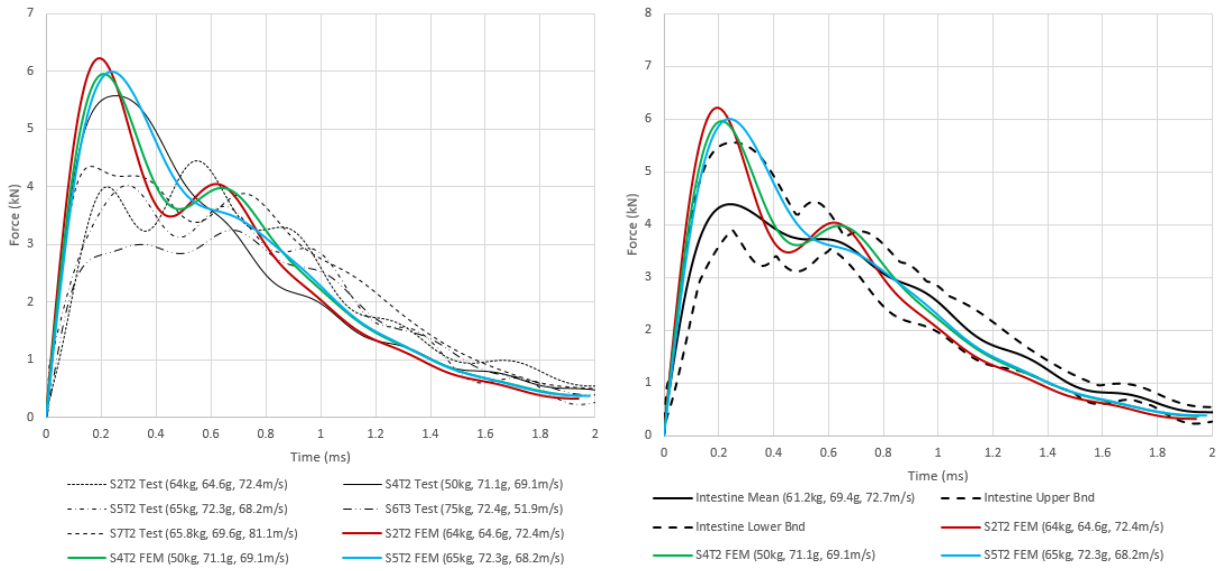

Figure 4-32. Comparison of force history between simulation and tests of intestine impact.

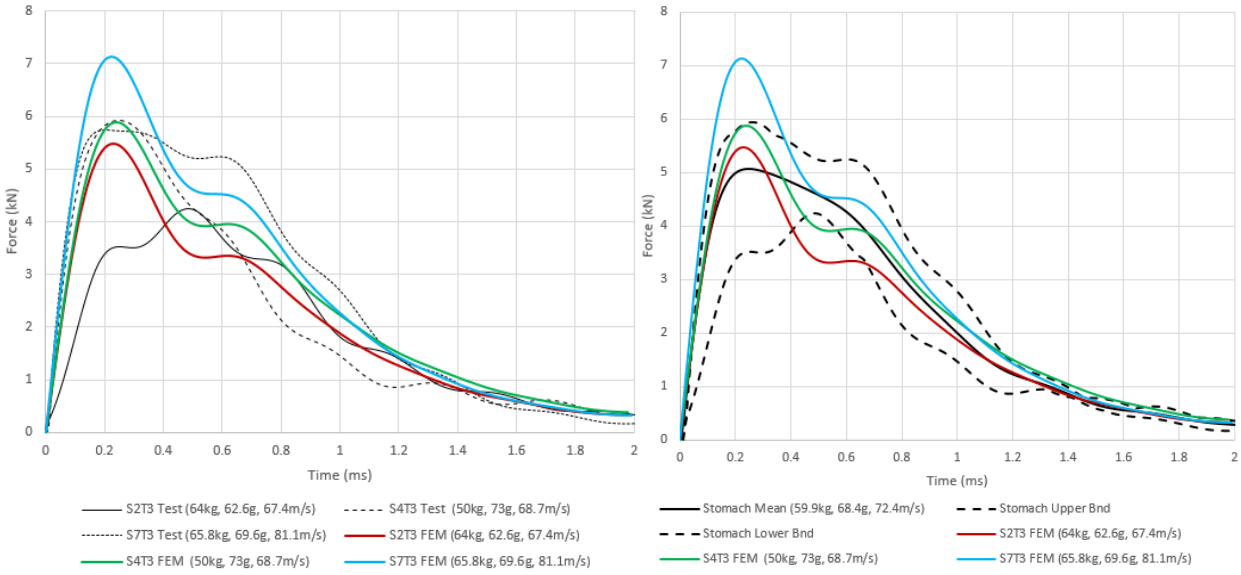

Figure 4-33. Comparison of force history between simulation and tests of intestine stomach.

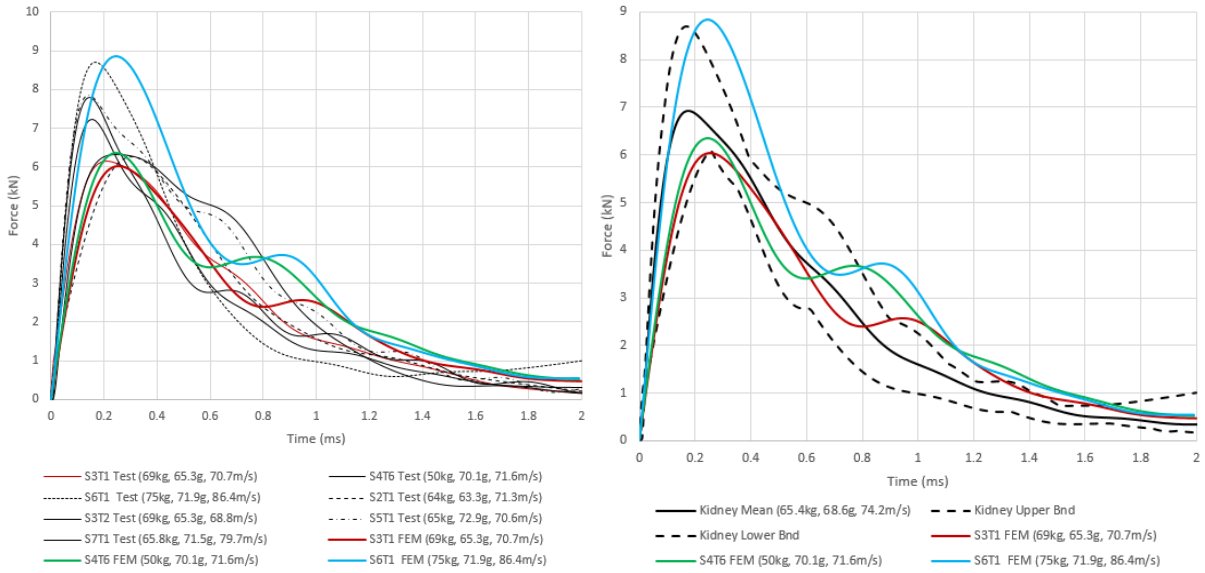

Figure 4-34. Comparison of force history between simulation and tests of intestine kidney.

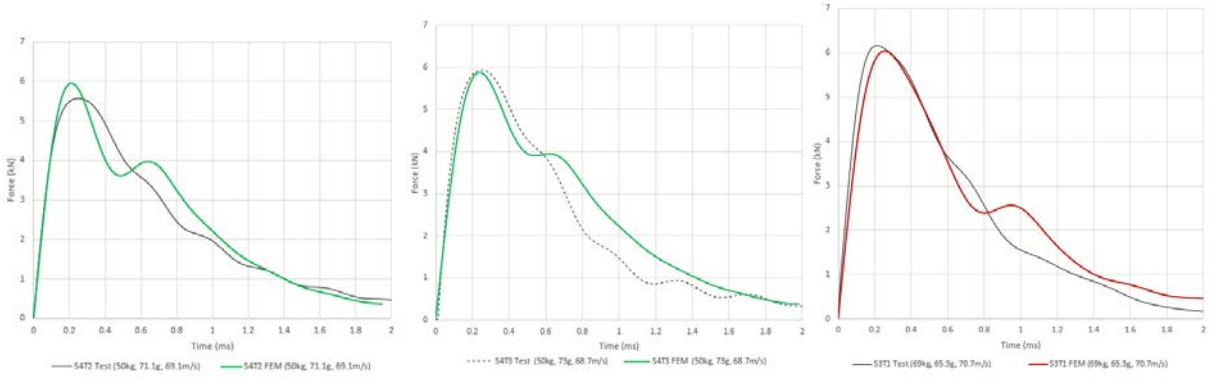

Figure 4-35. Force comparison of individual tests (intestine, stomach and kidney).

4.5.2 Simulation of John Hopkins APL PMHS Tests

Simulations of John Hopkins APL PMHS tests, described in Section 4.1.1.3, are conducted to validate the human torso FE model. The cylinder silicon projectile is assumed to be soft rubber and the material model, BLATZ-KO_RUBBER, with shear modulus 0.5MPa, is implemented. Simulation setups for both fleshed and defleshed are given in Figure 4-36, where the projectile impacted left rib#4 at speed 40m/s; for the defleshed test condition, the exterior tissue to the ribs is removed.

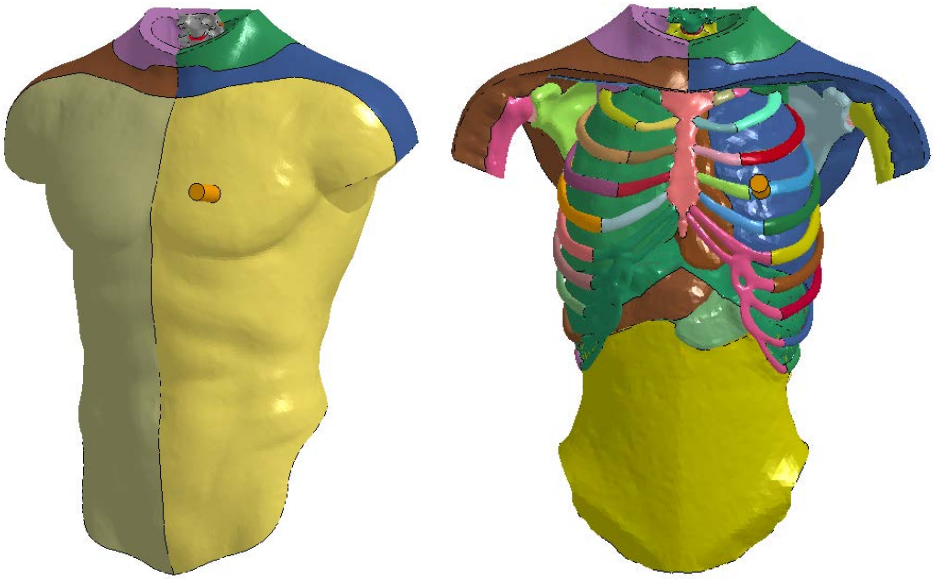

Figure 4-36. Simulations of fleshed and defleshed PMHS tests.

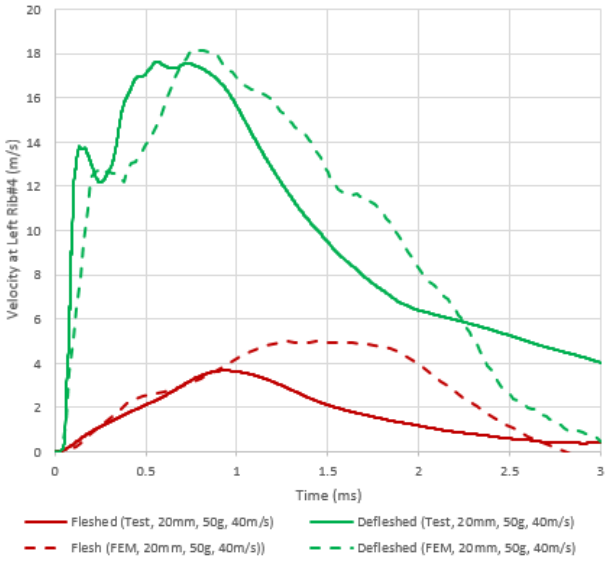

Figure 4-37. Comparison of velocity under rib#4 between tests and simulations.

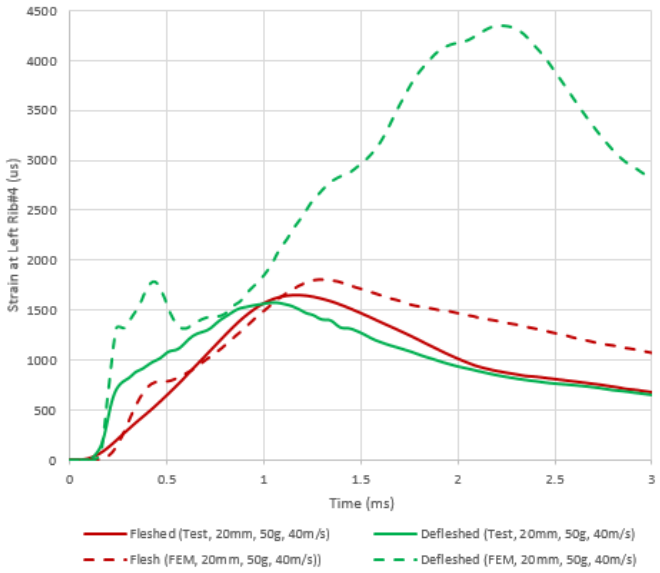

Figure 4-38. Strain comparison on rib#4 near impact location between tests and simulations.

The comparison of velocity under rib#4 is given in Figure 4-37. It can be seen that the simulated and measured velocities of defleshed test match very well, while the velocities from fleshed tests do not. The primary reason for this is that the test subject had a larger girth (more flesh) than the one used in the simulation model. The increased flesh severs as a pad and greatly reduces the velocity of rib. The strain comparison between tests and simulation are plotted in Figure 4-38. There are a lot uncertainties involved in testing and simulation, such as projectile material properties, test subject anatomy (flesh thickness), and location of strain gauge relative to the simulated point of impact. Thus the strain curves can only provide quantitative comparisons. Detailed comparisons are not available with the current testing details that were provided from Johns Hopkins APL.

4.5.3 Human Torso FEM Validation against Frontal Impact Tests

Frontal impact tests (Kroell, Schneider et al. (1971), (1974)) described in section 4.1.1.4 are be used to validate the overall structure stiffness of the torso FE model. The rigid pendulum striker impacts the frontal body region at the center of sternum, as depicted in Figure 4-39. The FE model size has been adjusted to match the weights of the test subjects. The mass and impact speeds are also adjusted to reflect the test conditions. The impact forces from the test measurements and simulations are plotted in Figure 4-37. Agreement between tests measurements and model simulations demonstrate that the human torso FEM performs well in calculation of mechanical responses to large impacts.

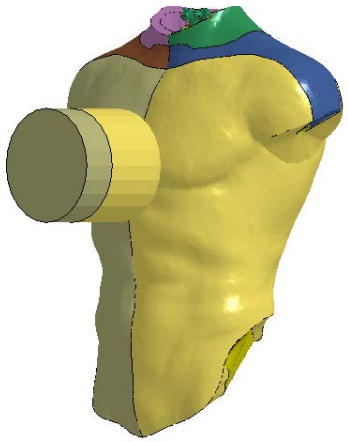

Figure 4-39. Simulation of frontal impact tests by pendulum striker.

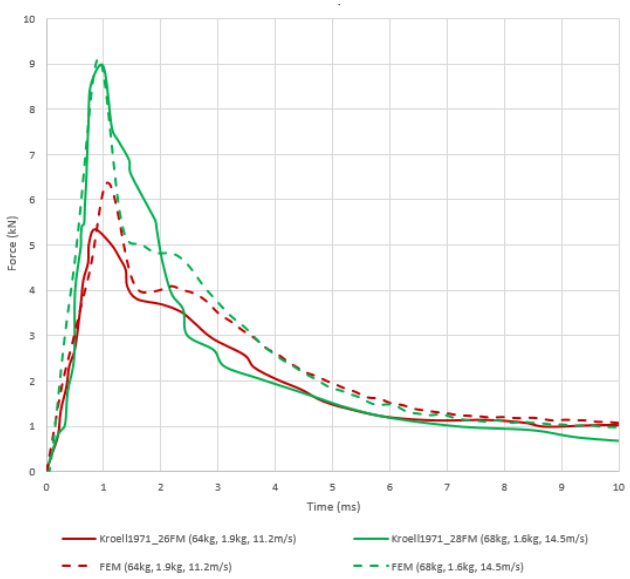

Figure 4-40. Comparison of impact between frontal impact tests and simulations.

4.5.4 Human Torso FEM Validation against Rear Impact Test

Simulation of a rear impact test (Forman, Perry et al. (2015)) (section 4.1.1.5) was conducted as a check of the back stiffness of the human torso model. The simulation setup is given in Figure 4-41 and the comparison of impact forces between test and simulation are plotted in Figure 4-42. It can be seen that the calculated force by model generally follows the trend of test data. Since, the impact speed is very low (5.5m/s) and the striker is very heavy (98kg), the reaction force is mainly effected by the structure stiffness instead of the local tissue properties. The structure stiffness is mainly determined by the spine model (joint connections between vertebrae, free rotation, etc.). The current spine is modeled as one continuous structure, which was developed for local deformation, and therefore maybe not be appropriate for simulation of overall structure behaviors.

Figure 4-41. Simulation of back impact.

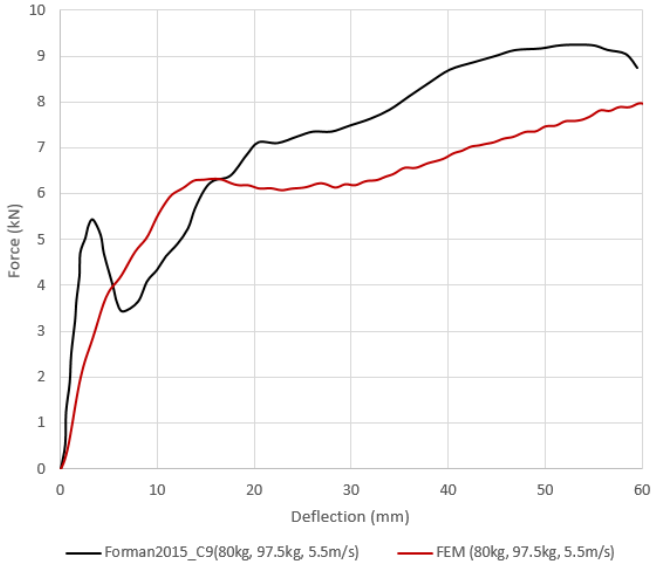

Figure 4-42. Comparison of impact Forces between rear impact test and simulation.

4.5.5 Back Injury Estimations of Animal Back Drop Tests

No back injury data from literature have been identified. Drop tests on animal backs are described in section 4.1.1.6 are used as quantitative estimations of back (spine) injuries. The reported injuries in Table 4-16 include vertebral fracture (spinous process fracture) and disc fracture (endplate fracture). Simulations of human torso FEM have been setup by following the two test conditions, as shown in Figure 4-41. The indictor values of vertebral fractures and disc fractures are given in Table 4-17. Comparing the thresholds of vertebral and disc fractures, both simulations predict the injury occurrences correctly. The tests are conducted on swine, while the simulations are on human model, so this is a very preliminary quantitative assessment.

Table 4-16. Animal back drop test configure and injury.

Test #	Drop mass (kg)	Velocity (m/s)	Location	Injury
2.1	28	4.2	T7/T8	Spinous process and endplate fracture
4.1	19.1	4.1	T8	Spinous process and endplate fracture

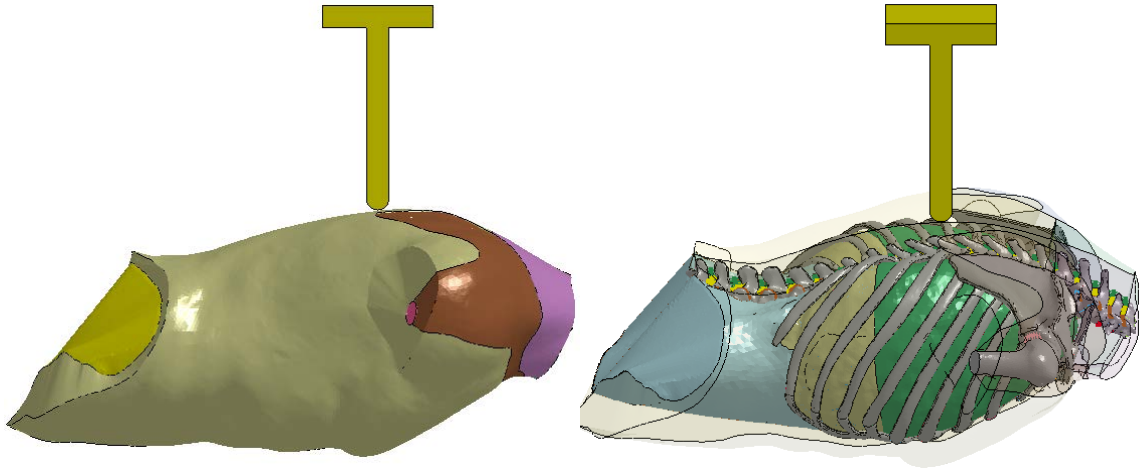

Figure 4-43. Simulations of Human torso FEM for back drop tests.

Table 4-17. Back injury estimation between animal tests and human model.

	Test 2.1	**Test 4.1**	**Threshold**
Vertebrae Cortical Bone VM-Stress (MPa)	142.2	163.9	112.7
Vertebrae Trabecular Bone VM-Stress (MPa)	5.35	4.87	4.8
Disc Annulus VM-Stress (MPa)	30.11	27.8	7.55
Predicted Vertebral Fracture (Y/N)	Y	Y	
Predicted Disc Fracture (Y/N)	Y	Y	

4.6 V&V Reporting Task Analysis

This subsection describes how the V&V activities were documented and what documentation was delivered.

The M&S was evaluated by L-3/ATI according to the V&V Plan completed in August 2018 (Niu and Ng 2018). The results of the evaluation are provided by L-3/ATI within this report under Contract No. N00174-17-C-0003.

5 V&V Issues

5.1 Limitation of Material models of Torso FEM

The material models used in the human torso FEM are listed in Table 4-8. The material of bone was simplified as one elastic model based on available test data, where any anisotropy, viscoelasticity and strain-rate dependence effects were not considered. The material model of liver, spleen, and kidney was selected as Ogden rubber and the material parameters were adjusted from compression simulation to satisfy the "mean" stress-strain curves from literature data (Section 4.2.3). The material model of body exterior was assumed to one homogenous rubber model and didn't consider the composite variations in different location around the body. The following issues were included in the setup of material models:

- Each internal organ material model was based on multiple sources and adopt the "mean" value;
- The material anisotropy was not considered;
- Body exterior tissues are assumed to have homogeneous tissue properties rather than discriminate composition differences;

5.2 Limitation of Implementation of Human Torso FEM

The developed FEM was used to predict blunt trauma under high speed projectiles. The impact assumes that the effects are localized to the torso region and the remainder of the body can be ignored.

As the deformations caused by the impact grow, the model is forced to delete elements to stay numerically stable. The model was found to remain stable to an extremely large impact loading. At faster speeds, large deformations will cause element deletion which can affect the model's predictions. In addition, the FEM has limited capability to calculate body motion which is dominated by the overall stiffness of the structure.

5.3 Limitation of Validation of FEM and Correlations

A comparison of the impact forces from the most recent and from historical PMHS testing was conducted. However, due to the difficulties in measuring internal response in addition to the inconsistency of the measurement itself, only comparison against rib strain was performed. Due to the multiple unknowns in testing and simulation, this study provides a first order assessment and comparison.

Similarly, back injury correlations cannot be developed due to absence of back impact dataset. Instead, a threshold-based comparison was made from tissue level failure strengths measured in static or quasistatic tests (tension, compression, or expansion). These values may be different under loading with a higher strain rate. Thus, the validation of injury correlation was more

qualitative in nature since the tests were conducted on animals and simulations were performed in human model.

6 Key Participants

This section identifies the participants involved in the VV&A effort, including the roles that they are assigned and their key responsibilities within that role. Roles and key responsibilities are defined during initial planning; names and contact information of the actual participants are added when they are determined.

6.1 Accreditation Participants

The accreditation roles of Accreditation Authority, Accreditation Agent, Accreditation Team, and SMEs have not yet been assigned.

6.2 V&V Participants

This subsection lists the participants involved in the V&V effort, including their contact information, assigned role, and the key responsibilities associated with that role. Typical V&V roles include M&S Proponent, V&V Agent, Validation Authority, Data Source, and SMEs.

Table 6-1. Participants in the V&V effort.

Level	Name	Company	Organization	Phone	E-mail
M&S Proponent		DoD	JNLWD		
M&S Developer	Eugene Niu/Laurel Ng	L-3	Applied Technologies, Inc.	(858) 404-7846	laurel.ng@L3T.com
V&V Agent	Eugene Niu/Laurel Ng	L-3	Applied Technologies, Inc.	(858) 404-7846	laurel.ng@L3T.com
Validation Authority	None assigned				
Data Source	None assigned				
SMEs	None assigned				

6.3 Other Participants

No other participants have been assigned at this time.

7 Actual V&V Resources Expended

This section discusses the resources expended during execution of the V&V Plan, such as performers, man-hours, materials, and funding. This information provides a mechanism to identify the impact of resource gaps on the current application and to scope resource requirements for future applications.

7.1 V&V Resources Expended

This subsection identifies the resources that were expended to accomplish the V&V activities. The information provided includes the activity, assigned performer, and the list of required resources.

V&V activities will be conducted by the M&S developer.

Model Verification:

SME review	2 man-months
Funding	$88K

Model Validation:

SME review	2 man-months
Funding	$88K

7.2 Actual V&V Milestones and Timeline

This subsection provides a chart of when the V&V milestones were achieved within the context of the overall program timeline (Table 7-1).

Table 7-1. Milestones and timeline to conduct V&V activities.

V&V Tasks	2018							
	April	May	June	July	Aug	Sept	Oct	Nov
FEM Development								
Injury Correlate Development								
Data Verification								
Data Validation								
Conceptual Model Validation								
Design Verification								
Implementation Verification								
Results Validation								
V&V Report								

A. APPENDIX: M&S DESCRIPTION

This appendix contains pertinent detailed information about the M&S being assessed.

A.1 M&S Overview

The M&S is a FEM of a 50th percentile male torso whose outputs are used to determine a probability of suffering a blunt trauma injury to the torso organs. The M&S is intended to predict the risk of blunt trauma injuries from kinetic energy non-lethal weapons such as rubber bullets and sponge grenades.

The geometry of the torso spans from the bottom neck (vertebrae C5) down to the middle waist (vertebrae L5) and was generated from the Zygote 3D Male Human Model (Zygote Media Group, American Fork, UT) based on CT scans of 50th percentile males. The tissues and organs are meshed with HyperMesh (Altair Hyperworks, Troy, MI).

Material properties are identified from a variety of literature sources where extensive testing of material properties had been performed and applied to the appropriate FEM parts. Appropriate contact parameters are established so that the model would have accurate force transmission between adjacent parts. Several formal model checks are performed throughout each step of the model's development and are outlined in detail in this report.

A.2 M&S Development and Structure

The completed FEM is a text file compatible with LS-Dyna. Once completed, the final structure, organization, hardware and software specifics (such as solver version), and technical statistics (such as runtime) can be provided. The paradigm being followed is a waterfall development process of sequential development steps. Figure 1 is an example of this development process, though the actual process will have additional V&V steps.

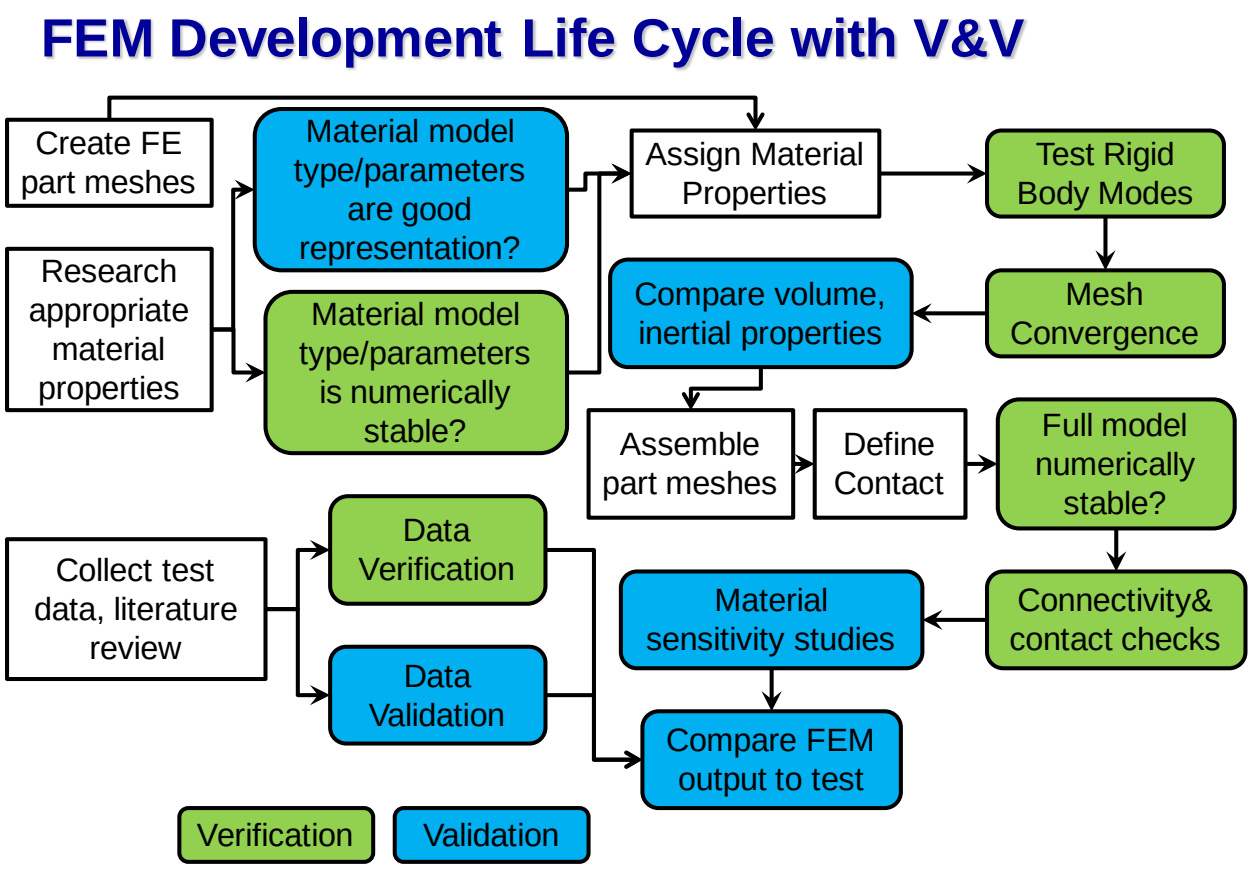

Figure A.2-1. An overview of the development cycle with V&V activities interspersed.

A.3 M&S Capabilities and Limitations

The M&S is intended to be a combination of a torso FEM and associated torso injury correlates. At this time, the M&S is still under development and therefore a complete list of its capabilities and limitations are not available.

A.4 M&S Use History

The M&S is still under development and has no use history at this time.

A.5 Data

A.5.1 Input Data

The input data necessary to run the M&S will be the necessary LS-Dyna files to run an impact simulation: the finished, unmodified torso FEM, a FEM of an impactor, the initial and boundary conditions, and the appropriate control settings to compute the appropriate simulation outputs. From these simulation outputs, the necessary data will be the logistic regressions that transform the FEM responses to injury probabilities.

A.5.2 Output Data

The M&S will produce intermediate outputs such as FEM responses like deformations, forces, stresses, and strains that will be necessary to compute the final outputs: injury probabilities. The FEM responses will be output in the same units as the FEM (SI units) and the probabilities will be given in percentages.

A.6 Configuration Management

Configuration management for the M&S will be conducted by the M&S developer. Any changes to the FEM, injury correlations, and V&V results will be reported in the M&S documentation (e.g., V&V report, change log).

M&S Role	Name	Company	Organization	Phone	E-mail
M&S Developer	Eugene Niu/Laurel Ng	L-3 Technologies	Applied Technologies, Inc.	(858) 404-7846	Laurel.ng@L3T.com

B. APPENDIX: M&S REQUIREMENTS TRACEABILITY MATRIX

This appendix establishes the links between the M&S requirements, the acceptability criteria, and the evidence collected during the V&V processes. Building on model requirement (Niu and Ng 2018) defined in Section 3.1, the traceability matrix provides a visual representation of the chain of information that evolves as the VV&A processes are implemented. As implementation progresses from the planning to reporting phases, the traceability matrix assists in the identification of information gaps that may result from VV&A activities neither performed, addressed, nor funded.

Table B-1. M&S requirements traceability matrix.

	Accreditation Plan		V&V Plan	V&V Report	Accreditation Report
#	M&S Requirement	Acceptability Criterion	Relevant V&V Task/Activity Section	V&V Task Analysis	Accreditation Assessment
1	Each sub-system will be meshed such that it contains the critical anatomical details necessary for accurate load transmission between adjacent sub-systems. Minor geometric details will be omitted (Anatomical geometry accuracy).	FE mesh of each organ/part must match reference geometry volume or area within 10%	4.2	4.2.1	
2	Each sub-system mesh resolution will be enough to ensure convergence of simulation results (Mesh convergence).	Volume percentage of peak mechanical responses (stress, strain, energy) match well those from finer mesh model.	4.3	4.3.2	
3	The material properties of the organs conform to the available test data within the deformation and strain-rate regimes of interest (Material model sensitivity)	Each organ's material model conforms with established stress-strain corridors from published test data	4.2	4.2.3	

4	Injury correlates shall be derived directly from the tissue mechanical responses of the associated sub-system (Injury correlation)	Ultimate strength will be directly used as a threshold to determine the injury, if sufficient data is not available to establish regressions	4.2	4.5.5	
5	No spatial penetration exists between sub-systems (Model construction & assembly)	Penetration due to mismatch of mesh resolution will be avoided be specifying appropriate contact formulations	4.4	4.4.1	
6	No big gaps between internal organs and chest wall, among contact organs (Model construction & assembly)	Adjust surface of internal organs to contact chest wall (no greater than 5% by volume)	4.4	4.2.1 4.4.1	
7	All contact and boundary conditions are properly initialized before the simulation (Model initialization)	The model has no internal energy at the beginning of the simulation	4.4	4.3.3	
8	Material model parameters proportionally affect simulation results (Model sensitivity)	20% perturbations in critical material property parameters result in a 20% or less proportional change in response	4.4	4.3.1	
9	Hourglass energy is minimal and limited throughout the simulation (Energy convergence)	Total hourglass energy less than 10% of the initial system energy in any test case	4.4	4.3.3	
10	Model maintains its integrity with minimal number of deleted elements due to excessive deformation (Model computational stability)	Fewer than 5% of elements deleted due to negative volume in all test cases	4.4	4.3.3	

11	Simulations of assembled model produce results comparable to those found in literature (Model validation)	Model compares favorably with published data of thorax dynamics caused by blunt impact, such as peak forces and deflection	4.5	4.5	
12	Model produces accurate injury outcomes (Correlation validation)	Injury predictions from simulations of tests match published data statistically	4.5	4.5.5	
13	Model based upon a 50% male but can be enlarged to a 95% male and reduced to a 5% male (Model adaptability & flexibility)	Simulation results from scaled models compare favorably with test data; computation completes within 150% runtime of 50% male model	4.5	4.5	

C. APPENDIX: BASIS OF COMPARISON

This appendix describes the basis of comparison used for validation. The basis for comparison serves as the reference against which the accuracy of the M&S representation is measured. The primary basis of comparison will come from comparisons with published data in peer-reviewed journals. Results from torso impacts performed on instrumented cadavers can be compared with M&S predictions made when simulating the impacts with the same boundary conditions. A secondary basis of comparison will be largely qualitative in nature, such as the injury patterns occurring in specific organ tissues.

The specifics of these comparisons (such as the methods, results, and assumptions) are undetermined at this time as the model is still under development. The results validation in the M&S V&V Report will provide a comprehensive overview of this information.

D. APPENDIX: REFERENCES

This appendix identifies all of the references used in the development of this document.

Arnoux, P. J., T. Serre, N. Cheynel, L. Thollon, M. Behr, P. Baque and C. Brunet (2008). "Liver injuries in frontal crash situations a coupled numerical - experimental approach." Comput Methods Biomech Biomed Engin **11**(2): 189-203.

Bass, D. C., R., K. A. Rafaels, R. S. Salzar, M. Carboni, R. W. Kent, M. D. Lloyd, S. Lucas, K. Meyerhoff, C. Planchak, A. Damon and G. T. Bass (2008). "Thoracic and lumbar spinal impact tolerance." Accident Analysis & Prevention **40**(2): 487-495.

Ben-Hatira, F., K. Saidane and A. Mrabet (2012). "A finite element modeling of the human lumbar unit including the spinal cord." Journal of Biomedical Science and Engineering **5**(3): 150.

Carter, F. J., T. G. Frank, P. J. Davies, D. McLean and A. Cuschieri (2001). "Measurements and modelling of the compliance of human and porcine organs." Med.Image Anal. **5**(4): 231-236.

Chawla, A., S. Mukherjee and B. Karthikeyan (2009). "Characterization of human passive muscles for impact loads using genetic algorithm and inverse finite element methods." Biomech Model Mechanobiol **8**(1): 67-76.

Egorov, V. I., I. V. Schastlivtsev, E. V. Prut, A. O. Baranov and R. A. Turusov (2002). "Mechanical properties of the human gastrointestinal tract." J Biomech **35**(10): 1417-1425.

Farshad, M., M. Barbezat, P. Flueler, F. Schmidlin, P. Graber and P. Niederer (1999). "Material characterization of the pig kidney in relation with the biomechanical analysis of renal trauma." J.Biomech. **32**(4): 417-425.

Forman, J., B. Perry, K. Henderson, J. P. Gjolaj, S. Heltzel, D. Lessley, P. Riley, R. Salzar and T. Walilko (2015). "Blunt impacts to the back: Biomechanical response for model development." Journal of Biomechanics **48**(12): 3219-3226.

Gao, Z., K. Lister and J. P. Desai (2010). "Constitutive Modeling of Liver Tissue: Experiment and Theory." Annals of biomedical engineering **38**(2): 505.

Granik, G. and I. Stein (1973). "Human ribs: Static testing as a promising medical application." Journal of Biomechanics **6**(3): 237-240.

Halldin, P. H., K. Brolin, S. Kleiven, H. von Holst, L. Jakobsson and C. Palmertz (2000). "Investigation of Conditions that Affect Neck Compression- Flexion Injuries Using Numerical Techniques." Stapp Car Crash J **44**: 127-138.

Hedenstierna, S. (2008). 3D Finite Element Modeling of Cervical Musculature and its Effect on Neck Injury Prevention. Ph.D., Royal Institute of Technology.

Karimi, A., M. Navidbakhsh, M. Alizadeh and A. Shojaei (2014). "A comparative study on the mechanical properties of the umbilical vein and umbilical artery under uniaxial loading." Artery Research **8**(2): 51-56.

Kemper, A., C. McNally, E. Kennedy, S. Manoogian and S. Duma (2007). The material properties of human tibia cortical bone in tension and compression: Implications for the tibia index. In Proceedings of the 20th Enhanced Safety of Vehicles Conference,, Lyon, France

Kemper, A., A. Santago, J. Sparks, C. Thor, C. H. Gabler, J. Stitzel and S. Duma (2011). Multi-scale biomechanical characterization of human liver and spleen. Proceedings of the 22nd International Technical Conference on the Enhanced Safety of Vehicles (ESV). Washington, DC.

Kemper, A. R., C. McNally, E. A. Kennedy, S. J. Manoogian, A. L. Rath, T. P. Ng, J. D. Stitzel, E. P. Smith, S. M. Duma and F. Matsuoka (2005). "Material properties of human rib cortical bone from dynamic tension coupon testing." Stapp Car Crash J **49**: 199-230.

Kemper, A. R., A. C. Santago, J. D. Stitzel, J. L. Sparks and S. M. Duma (2012). "Biomechanical response of human spleen in tensile loading." Journal of Biomechanics **45**(2): 348-355.

Kimpara, H. (2015). INVESTIGATION OF SERIOUS–FATAL INJURIES USING BIOMECHANICAL FINITE ELEMENT MODELS. Ph.D. Doctor of Engineering, Nagoya University.

Kroell, C. K., D. C. Schneider and A. M. Nahum (1971). Impact tolerance and response of the human thorax. Proc 15th Stapp Car Crash Conference, SAE International. **15:** 84-134.

Kroell, C. K., D. C. Schneider and A. M. Nahum (1974). Impact Tolerance and Response of the Human Thorax II. Proc 18th Stapp Car Crash Conference, SAE International. **18:** 383-457.

Kumaresan, S., N. Yoganandan, F. A. Pintar and D. J. Maiman (1999). "Finite element modeling of the cervical spine: role of intervertebral disc under axial and eccentric loads." Medical Engineering and Physics **21** 689-700.

Li, Z., M. W. Kindig, J. R. Kerrigan, C. D. Untaroiu, D. Subit, J. R. Crandall and R. W. Kent (2010). "Rib fractures under anterior-posterior dynamic loads: experimental and finite-element study." J Biomech **43**(2): 228-234.

Li, Z., M. W. Kindig, D. Subit and R. W. Kent (2010). "Influence of mesh density, cortical thickness and material properties on human rib fracture prediction." Med Eng Phys **32**(9): 998-1008.

Lizee, E., S. Robin, E. Song, N. Bertholon, J.-Y. L. Coz, B. Besnault and F. Lavaste (1998). "Development of a 3D finite element model of the human body." SAE Stapp Car Crash Conference Proceedings **983152**.

Mathews, K. and C. Webber (2017). Test Report for PMHS Validation Testing. San Diego, California, L-3 Applied Technologies, Inc.

Meyer, F., N. Bourdet, C. Deck, R. Willinger and J. S. Raul (2004). "Human Neck Finite Element Model Development and Validation against Original Experimental Data." Stapp Car Crash J **48**: 177-206.

Niu, E. and L. Ng (2018). Design Requirements Specification ATBM Thorax Model. San Diego, California, L-3 Applied Technologies, Inc.

Niu, E. and L. Ng (2018). Verification and Validation Plan for ATBM-Torso Finite Element Modeling and Injury Correlation. San Diego, California L-3 Applied Technologies, Inc.

Noailly, J., L. Ambrosio, K. Elizabeth Tanner, J. A. Planell and D. Lacroix (2012). "In silico evaluation of a new composite disc substitute with a L3-L5 lumbar spine finite element model." Eur Spine J **21 Suppl 5**: S675-687.

Reilly, D. T. and A. H. Burstein (1975). "The elastic and ultimate properties of compact bone tissue." J Biomech **8**(6): 393-405.

Roberts, J. C., A. C. Merkle, P. J. Biermann, E. E. Ward, B. G. Carkhuff, R. P. Cain and J. V. O'Connor (2007). "Computational and experimental models of the human torso for non-penetrating ballistic impact." Journal of Biomechanics **40**(1): 125-136.

Rosen, J., J. D. Brown, S. De, M. Sinanan and B. Hannaford (2008). "Biomechanical properties of abdominal organs in vivo and postmortem under compression loads." Journal of Biomechanical Engineering **130**(2): 021020.

Safshekan, F., M. Tafazzoli-Shadpour, M. Abdouss and M. Shadmehr (2016). "Mechanical Characterization and Constitutive Modeling of Human Trachea: Age and Gender Dependency." Materials **9**(6): 456.

Shen, W. and Y. Niu (2008). "Development and Vallidation of Subject-Specific Finite Element Models for Blunt Trauma Study." Journal of Biomechanical Engineering **130**: 021022-021021-021022-021021.

Shigeta, K., Y. Kitagawa and T. Yasuki (2009). Development of Next Generation Human Body FE Model Capable of Organ Injury Prediction. Proceedings: International Technical Conference on the Enhanced Safety of Vehicles, National Highway Traffic Safety Administration. **2009**.

Snedeker, J. G., M. Barbezat, P. Niederer, F. R. Schmidlin and M. Farshad (2005). "Strain energy density as a rupture criterion for the kidney: impact tests on porcine organs, finite element simulation, and a baseline comparison between human and porcine tissues." Journal of Biomechanics **38**(5): 993-1001.

Song, B., W. Chen, Y. Ge and T. Weerasooriya (2007). "Dynamic and quasi-static compressive response of porcine muscle." Journal of Biomechanics **40**(13): 2999-3005.

Sparks, J. L. (2007). Biomechanics of Blunt Liver Injury: relating internal pressure to injury severity and developing a constitutive model of stress-strain behavior. Ph.D., The Ohio State University.

Stein, I. and G. Granik (1976). "Rib structure and bending strength: an autopsy study." Calcified tissue research **20**(1): 61-73.

Stitzel, J. D., J. M. Cormier, J. T. Barretta, E. A. Kennedy, E. P. Smith, A. L. Rath, S. M. Duma and F. Matsuoka (2003). "Defining regional variation in the material properties of human rib cortical bone and its effect on fracture prediction." Stapp Car Crash J **47**: 243-265.

Subit, D., E. d. P. de Dios, J. Valazquez-Ameijide, C. Arregui-Dalmases and J. Crandall (2011). "Tensile material properties of human rib cortical bone under quasi-static and dynamic failure loading and influence of the bone microstucture on failure characteristics." arXiv preprint arXiv:1108.0390.

Tamura, A., K. Omori, K. Miki, J. B. lee, K. H. Yang and A. I. King (2002). "Mechanical characterization of Porcine abdominal organs." The Stapp Car Crash Journal **46**(Paper No. 2002-22-0003): 53-69.

Umale, S., C. Deck, N. Bourdet, P. Dhumane, L. Soler, J. Marescaux and R. Willinger (2012). "Experimental mechanical characterization of abdominal organs: liver, kidney & spleen." Journal of the Mechanical Behavior of Biomedical Materials **17**: 22-33.

Vannah, W. M. and D. S. Childress (1996). "Indentor tests and finite element modeling of bulk muscular tissue in vivo." J.Rehabil.Res.Dev. **33**(3): 239-252.

Webber, C., Y. Niu and K. Mathews (2017). Literature Review of Neck Traumatology, Properties, Modeling Methods, and Injury Studies. San Diego. CA, L-3 Applied Technologies, Inc.

Yamada, H. (1970). Strength of Biological Materials. Baltimore, The Williams & Wilkins Company.

Yoganandan, N., S. Kumaresan and F. A. Pintar (2001). "Biomechanics of the cervical spine Part 2. Cervical spine soft tissue responses and biomechanical modeling." Clin.Biomech.(Bristol., Avon.) **16**(1): 1-27.

Zhao, J. and G. Narwani (2005). Development of a Human Body Finite Element Model for Restraint System R and D Applications. Proceedings: International Technical Conference on the Enhanced Safety of Vehicles, National Highway Traffic Safety Administration. **2005:** 13p-13p.

Zhao, J. Z. and G. Narwani (2007). Biomechanical Analysis of Hard Tissue Responses and Injuries with Finite Element Full Human Body Model. ESV 07-0354.

Zhu, Y., F. Bermond, J. Payen de la Garanderie, J.-B. Pialat, B. Sandoz, D. Brizard, J.-P. Pracros, F. Rongieras, W. Skalli and D. Mitton (2017). "In Vivo Assessment of Elasticity of Child Rib Cortical Bone Using Quantitative Computed Tomography." Applied Bionics and Biomechanics **2017**: 9.

E. APPENDIX: ACRONYMS

This appendix identifies all acronyms used in this document.

ATBM	Advanced Total Body Model
DT&E	Development Test and Evaluation
FEM	Finite Element Model
HECOE	Human Effects Center of Excellence
JNLWD	Joint Non-Lethal Weapons Directorate
JNLWP	Joint Non-Lethal Weapon Program
M&S	Modeling and Simulation
MOE	Measures of Effectiveness
MOP	Measures of Performance
MOS	Measures of Suitability
NLWs	Non-Lethal Weapons
OT&E	Operational Test and Evaluation
PMHS	Post-Mortem Human Subject
SME	Subject Matter Expert
V&V	Verification and Validation
V50	Model response at which injury is 50% likely
VV&A	Verification, Validation, and Accreditation

F. APPENDIX: GLOSSARY

This appendix contains definitions that aid in the understanding of this document.

ACCEPTABILITY CRITERIA. A set of standards that an M&S must meet to be accredited for a specific purpose.

ACCREDITATION. The official certification that an M&S and its associated data are acceptable for use for a specific purpose.

ACCREDITATION AGENT. The individual, group, or organization designated by the Accreditation Authority to conduct an accreditation assessment for an M&S.

ACCREDITATION AUTHORITY. The organization/individual who approves the use of an M&S for a particular application.

CONCEPTUAL MODEL. The developer's description of what the model or simulation will represent, the assumptions limiting those representations, and other capabilities needed to satisfy the M&S User's requirements. A collection of assumptions, algorithms, relationships, and data that describe a developer's concept about the simulation.

DATA. A representation of facts, concepts, or instructions in a formalized manner suitable for communication, interpretation, or processing by humans or by automatic means. Assumed, given, measured, or otherwise determined facts or propositions used to draw a conclusion or make a decision.

DATA VERIFICATION AND VALIDATION. The process of verifying the internal consistency and correctness of data and validating that it represents real world entities appropriate for its intended purpose or an expected range of purposes.

INDEPENDENT REVIEW. In computer modeling and simulation, a review performed by competent, objective reviewers who are independent of the model developer. Independent review includes either: (a) a detailed verification and/or validation of the model or simulation; or (b) an examination of the verification and/or validation performed by the model or simulation developer.

INTENDED USE. The application of a model or simulation for a specific purpose.

M&S DEVELOPER. The individual, group or organization responsible for developing or modifying a simulation in accordance with a set of design requirements and specifications.

M&S PROPONENT. The organization that has primary responsibility for M&S planning and management that includes development, verification and validation, configuration management, maintenance, use of an M&S, and others as appropriate.

M&S LIFECYCLE. The period of time beginning when an M&S product is conceived and ending when the product is no longer available for use. The M&S lifecycle is typically broken into phases, such as requirements definition, design, development, test, and operation and maintenance.

M&S REQUIREMENTS. The collection of requirements that an M&S must meet to serve a particular purpose. M&S requirements include problem, M&S User, and simulation domain requirements.

M&S USER. The individual, group, or organization that uses the results or products from a specific application of an M&S. The M&S User is a Government entity.

REQUIREMENTS TRACEABILITY. The degree to which a relationship can be established between the M&S requirements, associated acceptability criteria for accreditation, and evidence collected during verification and validation implementation.

SIMULATION DOMAIN. Aspects of an M&S related to the implementation environment (e.g., time management, object interaction control, M&S User interfaces, databases, and report generators).

SUBJECT MATTER EXPERT. An individual who, by virtue of education, training, or experience, has expertise in a particular technical or operational discipline, system, or process.

M&S USER DOMAIN. The realm of knowledge describing an M&S User's environment to which an M&S will be applied.

VALIDATION. The process of determining the degree to which an M&S and its associated data are an accurate representation of the real world from the perspective of the intended uses of the model. The process of determining the fitness of an M&S and its associated data for a specific purpose.

VERIFICATION. The process of determining that an M&S implementation and its associated data accurately represent the developer's conceptual description and specifications. The process of determining that an M&S faithfully represents the developer's conceptual description and specifications. Verification evaluates the extent to which the M&S has been developed using sound and established software and system engineering techniques.

VERIFICATION AND VALIDATION (V&V) AGENT. The individual, group, or organization designated by the M&S Proponent to verify and validate an M&S. The V&V agent provides information to the Accreditation Agent to support the recommendation to accredit an M&S for a specific purpose. The organization designated by the M&S Proponent to perform verification and validation of an M&S.

G. APPENDIX: V&V PROGRAMMATICS

This appendix contains detailed information regarding resource allocation and funding (Table G-1).

Table G-1. Estimated resources needed for V&V activities.

Actual Resource Allocations and Funding			
V&V Activity	**Required Resources**	**Funding Source**	**FY18 $K**
Verification by M&S Developer	$88k	JNLWD	$88k
Validation by M&S Developer	$88k	JNLWD	$88k

H. APPENDIX: DISTRIBUTION LIST

This appendix provides the distribution list for hardcopies or digital copies of the approved document.

Joint Non-Lethal Weapons Directorate (1)